Multidecadal trends in CO_2 evasion and aquatic metabolism in a large temperate river

An Truong Nguyen[1*], Gwenaël Abril[2,3], Jacob S. Diamond[1,4], Raphaël Lamouroux[5], Cécile Martinet[6], Florentina Moatar[1]

[1] INRAE, UR RiverLy, 5 Rue de la Doua, 69100 Villeurbanne, France

[2] Laboratoire de Biologie des Organismes et Ecosystèmes Aquatiques (BOREA), UMR 8067, Muséum National d'Histoire Naturelle, CNRS, IRD, SU, UCN, UA, Paris, France.

[3] Programa de Geoquímica, Universidade Federal Fluminense, Niterói, Rio de Janeiro, Brazil

[4] Dipartimento di Scienze Ambientali, Informatica e Statistica, University of Venice Ca' Foscari, Via Torino 155, 30172 Venezia Mestre, Italy

[5] EDF – Recherche et Développement, Laboratoire National d'Hydraulique et Environnement, Chatou, France

[6] EDF – Division Technique Générale, Electricité de France, Grenoble, France

[*] Corresponding author: truongan9393@yahoo.com

Abstract. Rivers play a critical role in the global carbon cycle. However, the environmental and hydro-climatic factors that control the sign and magnitude of river CO_2 fluxes across seasons and multidecadal periods are less constrained. The origin of excess river CO_2—delivered by soils, wetlands and groundwater or produced by aquatic respiration of organic matter—remains an important unknown in linking terrestrial and aquatic carbon budgets. To address these knowledge gaps, we report on a 32-year high-frequency dataset (1990–2021) from the Loire River, a large, temperate river that underwent a shift from a phytoplankton-dominated regime to a macrophyte-dominated regime in ca. 2005. We estimated daily river-atmosphere CO_2 flux (FCO_2) and river net ecosystem productivity (NEP) from hourly pH, alkalinity, dissolved oxygen, water temperature and solar radiation. We demonstrate that: i) annual FCO_2 varied an order of magnitude among years (range = 200–2600 g C m^2 yr^{-1}) with a long-term decrease trend, mainly linked to decreased groundwater contribution; ii) the mean annual contribution of aquatic metabolism to total FCO_2 was 40%, increasing from 37 ± 27% in phytoplankton-dominated regime to 57 ± 10% in macrophyte-dominated regime; iii) while the river predominantly acted as a CO_2 source, it occasionally functioned as a CO_2 sink ($FCO_2 < 0$) during summer, though this sink behavior constituted a minor component (-0.6%) of the FCO_2 budget; and iv) FCO_2 exhibited strong seasonality linked to discharge, exhibiting hysteresis where FCO_2 levels at equivalent discharge were 1.5 to 2 times higher

during the rising limb (autumn) compared to the falling limb (spring). The magnitude of this hysteresis diminished in the later macrophyte-dominated regime, indicating a changing seasonal discharge control. This study makes clear that river FCO_2—and its source—is dynamic within and across years, driven by hydro-climatic variations and biological activity. Catchment-scale hydrogeological changes can be a more dominant driver of long-term riverine CO_2 evasion than in-stream ecological regime shifts, controlling the balance between internal and external CO_2 production.

Keywords: internal contribution, autotrophic, heterotrophic, long-term trend, metabolic shift, Loire River

1. Introduction

Streams and rivers are a major component of inland water CO_2 evasion, with the most recent estimates for this flux at 2.0 ± 0.2 Pg C yr^{-1} (Liu et al., 2022). Earlier foundational work suggested this riverine flux accounted for approximately 60% of all inland waters (Raymond et al., 2013). Most CO_2 flux (FCO_2) is often assumed to come from "external" sources, delivered to streams via groundwater inputs and via temporary hydrologic connectivity with riparian wetlands (Abril & Borges, 2019; Hotchkiss et al., 2015). Additional, geochemical weathering and photochemical processes are also considered external sources to river FCO_2 (Hotchkiss et al., 2015). While geochemical weathering primarily affects river alkalinity and indirectly influences CO_2 dynamics through changes in water chemistry (J. B. Jones et al., 2003), photochemical processes make a relatively minor contribution to CO_2 production when compared to biological processes (Amaral et al., 2013; Koehler et al., 2014). The remainder of FCO_2 from rivers originates from in-stream respiration of organic matter (Cole et al., 2001), termed the "internal" source of CO_2. While the balance between internal versus external CO_2 sources is spatially predictable (Hotchkiss et al., 2015), its temporal variation is less clear. Most analyses on the origin of stream FCO_2 occur over one season (e.g., Bernal et al., 2022; Rocher-Ros et al., 2020) or rely on discrete samplings (e.g., Hotchkiss et al., 2015). Consequently, while progress has been made, a comprehensive understanding of the full spectrum of temporal variability (seasonal to multidecadal) in FCO2 and its sources remains limited, particularly for large river systems. Recent work by Young et al. (2025) highlighted this complexity by documenting strong seasonal variability driven by hydrological events, temperature fluctuations, and biological productivity in a temperate river. Their four-year study

emphasized the need for longer-term datasets to capture interannual variability, particularly in the context of ongoing climate and ecological changes. The seasonal hydrology plays an important role in determining the magnitude and timing of CO_2 emissions from rivers, as changes in flow rates affect the transport of nutrient, organic carbon from surrounding land as input for stream metabolism and the exchange of CO_2 between the river and the atmosphere (Cole et al., 2007; Hotchkiss et al., 2015). There is thus a lack of understanding of the temporal variability of FCO_2 and its sources, which are increasingly crucial under a changing climate that increases water temperature and modifies river flow (Floury et al., 2012; Van Vliet et al., 2013). This knowledge gap is most prominent in large rivers, leading to significant uncertainty in global FCO_2 assessment from inland waters (Battin et al., 2023; Hotchkiss et al., 2015).

The relative contribution of internal CO_2 sources can be quantified as the ratio between net ecosystem productivity (NEP) and FCO_2. NEP is the balance between gross primary production (GPP) and ecosystem respiration (ER) (NEP = GPP – ER). When NEP is negative (GPP < ER), the river is in a "heterotrophic" state, and CO_2 is added to the water column by net organic matter respiration. Assuming the river is a CO_2 source ($FCO_2 > 0$) and in a heterotrophic state, the $-NEP/FCO_2$ ratio yields the ratio of internal source contribution to total emissions, and by difference, the ratio of external CO_2 source contribution ($=1+ NEP/FCO_2$). This ratio can be evaluated in response to environmental drivers such as hydrology (Hotchkiss et al., 2015), light (Rocher-Ros et al., 2021), water temperature (Lynch et al., 2010; Wallin et al., 2020), and organic matter source (Bernal et al., 2022; Reed et al., 2021). However, rivers are not always CO_2 sources and can seasonally function as CO_2 sinks when high rates of GPP deplete CO_2, leading to CO_2 undersaturation (Aho et al., 2021; Zhang et al., 2017). In this "autotrophic" state (GPP > ER), positive NEP means a net production of organic matter within the reach, leading to increases in biomass (e.g., algal, macrophyte) and potentially contributing to particulate and dissolved organic matter pools. Such autotrophic state, sometimes leading to CO_2 undersaturation, can be more prevalent or sustained in larger rivers due to factors like greater water residence times, increased light availability across wider channels, and potentially a greater buffering capacity against rapid changes in external CO_2 inputs compared to smaller streams (Hotchkiss et al., 2015). However, these periods, especially if transient or occurring outside of typical low-flow summer conditions, can be missed FCO_2

sampling campaigns that are often infrequent or biased towards specific seasons, thus underestimating their occurrence and impact.

The eutrophic state was common in large rivers throughout the 1980s and 1990s, characterized by high nutrient concentrations and high chlorophyll-*a*, leading to a net autotrophic state (Dodds & Smith, 2016). The Loire River (France) was one of the most eutrophic rivers in Europe at that time with total phosphorus (TP) concentrations frequently exceeding 0.2 mg P L^{-1} and chlorophyll-a concentrations often surpassing 100 µg L^{-1}, with summer peaks reaching over 200 µg L^{-1} (Minaudo et al., 2015; Moatar & Meybeck, 2005). Despite potential autotrophic activity, the CO_2 dynamics during these periods remains poorly documented due to the lack of comprehensive CO_2 data, leaving a gap in our understanding of whether the river predominantly acted as a CO_2 source or sink.

Following efforts to reduce nutrient inputs between the early 1990s and the mid-2000s, TP concentrations declined by approximately 50-70%, and mean summer chlorophyll-a concentrations decreased to <30 µg L^{-1} (Minaudo et al., 2015). The Loire River underwent ecological shifts from planktonic autotrophic communities dominated by phytoplankton to benthic communities dominated by rooted macrophytes (Minaudo et al., 2015), which is termed "re-oligotrophication" (Ibáñez et al., 2022). The ecosystem transition was followed by a delayed shift in the river's metabolic regime around 2012–2014, with GPP declining and NEP decreasing by roughly 10% during the spring–summer growing season (Diamond et al., 2022). As re-oligotrophication may become increasingly common in developed countries, its effects on FCO_2 and CO_2 source variation remain unknown.

In this study, we used a 32-year daily dataset of coupled stream metabolism (NEP) and FCO_2 to assess the temporal internal/external CO_2 source contributions in the Loire River. We hypothesized that the FCO_2 and its internal source contribution would increase following the re-oligotrophication ecosystem shift. Specifically, we predicted that these increases would manifest coincidentally with the shifts in phytoplankton to macrophyte-dominated regime in 2005 and stream metabolism regime in 2012. Finally, discharge influences FCO_2 through multiple mechanisms, including gas transfer velocity, delivery of external CO_2, and inhibition of in-stream primary production. Phytoplankton GPP can be sensitive to discharge (e.g., washout, turbidity), while macrophyte GPP may be less directly flow-

dependent (Diamond et al., 2022). We therefore predicted that the overall control of discharge (Q) on FCO2 would change with the shift to macrophyte dominance. Specifically, we anticipated that the seasonal hysteresis patterns observed in the FCO_2-Q relationship (where FCO_2 differs between rising and falling limbs of the hydrograph at similar Q) would be altered, potentially becoming less pronounced or showing a different shape if macrophyte GPP imparts a more stable baseline of CO_2 uptake across varying flow conditions compared to phytoplankton.

2. Methods

2.1. Study site

The study site (47.6°N, 2.6°E) is located in the middle Loire River, France, 564 km from the source, with a mean discharge of 300 $m^3 s^{-1}$ (Supplementary Figure S1). Its 36,000 km^2 catchment is home to over two million residents. The land cover consists of forests (42%), pasture (35%), and agriculture (21%) (Moatar & Meybeck, 2005). The Loire River and its tributaries, upstream Dampierre drains volcanic, granitic area and sedimentary basins characterized by extensive limestone and marl formations (Figure S1). After the confluence with Allier River (100 km upstream of the study site), the carbonate-rich catchment and its interaction with the Loire River significantly contribute to river alkalinity primarily through the dissolution of carbonate minerals (Binet et al., 2022). Soil types within the Loire catchment are heterogeneous and their nature is closely linked to the underlying lithology. In addition, the catchment includes significant areas of alluvial deposits, which feature more fertile and productive soils for extensive agriculture in the region (Moatar et al., 2022; Moatar & Meybeck, 2005). This river is an 8^{th}-order river with an anabranching fluvial pattern resulting from a gentle slope (0.4 m km^{-1}). During summer, low flows (<150 $m^3 s^{-1}$), the study site is typically shallow (around 1 m deep) and wide (330 m); during winter, with higher discharges (e.g., >500 $m^3 s^{-1}$), depths can increase significantly, typically ranging from 2 to 3 m. The anabranching fluvial pattern leads to a broad range of lateral hydrologic connectivity between the main channel and secondary channels colonized by semi-terrestrial vegetation (Janssen et al., 2023). These vegetated side channels may behave like floodplains by acting as seasonal sources of organic carbon (Abril & Borges, 2019).

2.2. Data acquisition and processing

Hourly data of pH, temperature, electrical conductivity (EC) at 25°C, and dissolved oxygen (DO) from 1990–2021 were extracted from the monitoring program conducted by Électricité de France (EDF) upstream and downstream of the nuclear power plant Dampierre (47.6°N, 2.6°E) (Figure S2). Total alkalinity (TA) was obtained from grab samples collected by both EDF and the Loire-Brittany Water Agency (AELB), with measurement frequency ranging from daily to monthly. We reconstructed a continuous daily TA time series from the relationship between EC and TA (Appendix A, Figure A2). This study used the upstream data to calculate daily FCO_2 and NEP, while the downstream data was used to support the data cleaning procedure. A full description of the data acquisition, quality control framework, and data processing is available in **Appendix A**.

We obtained daily global radiation data (W m^{-2}) from a nearby meteorological station (donneespubliques.meteofrance.fr). Mean daily discharge (m^3 s^{-1}) was obtained from www.hydro.eaufrance.fr. We then estimated average river depth (m) using a local rating curve (Depth (m)=0.0716×√(Q (m^3 s^{-1}) + 0.6171), which was established based on the hydraulic model for the Loire River (Camenen et al., 2016).

2.3. NEP and FCO_2 estimation

2.3.1. Metabolism estimation

We estimated daily GPP, ER (g O_2 m^{-2} d^{-1}), and the gas exchange rate coefficient (K_{600}, d^{-1}) by using the inverse modelling approach that yields the best fit between modeled and observed DO. To avoid the unrealistic estimates, the K_{600} is constrained by daily river discharge and river depth with the formulations proposed by Raymond et al., 2012, while the hourly DO, solar radiation and daily water temperature data are required to further reduce equifinality of GPP, ER and K_{600}. These estimates are supported by the *streamMetabolizer*, a R package (Appling et al., 2018). The model setup for the Loire River was described by Diamond et al. (2021) and Diamond et al. (2025). GPP and ER were then converted to carbon units (g C m^{-2} d^{-1}) using a fixed molar O_2:C ratio of 1:1. This assumption is widely used in river metabolism studies and reflects the stoichiometry of aerobic metabolism (Trentman et al., 2023). Although photosynthetic and respiratory quotients (PQ and RQ) can vary with autotrophic community composition, recent long-term analysis of the Loire River by Diamond et al. (2025) showed that such variability does not lead to cumulative bias in net ecosystem production or CO_2 budgets when integrated over decadal timescales. Therefore, we adopt this approach as a reasonable and conservative approximation for estimating long-term carbon dynamics, while acknowledging it as a source of short-term uncertainty.

About 12% of samples (n=1391) were discarded due to physically impossible results in metabolism estimation (i.e., negative values). Missing mean daily GPP and ER were then replaced by their daily 75th estimated percentile values provided by *streamMetabolizer*, as detailed in **Appendix B, Section B1**. We imputed the remaining 1.7% of missing data using the rolling 7-day average. The K_{600} values derived from the model were validated against established empirical equations and found to be of the same order of magnitude, as detailed in **Appendix B, Section B2**. The covariance between estimated ER and K600 was low ($R^2 = 0.09$), demonstrating reduced influence of equifinality problem (Appling et al., 2018).

2.3.2. pCO_2 and FCO_2 estimation

Daily concentrations of partial pressure of CO_2 (pCO_2, µatm) were estimated by pyCO2SYS, a Python package for the CO2SYS model (Humphreys et al., 2022), using mean daily pH, water temperature, and TA. Carbonate dissociation constants K_1 and K_2 were chosen based on freshwater estimates (Millero, 1979). CO2SYS freshwater pCO_2 estimates are valid for water with TA > 1000 µmol L^{-1}, and results have been previously validated for the Loire River (2–9% bias) (Abril et al., 2015). The daily TA data in this study were estimated from daily EC with an average error of 190 µmol L^{-1}, leading to an uncertainty in pCO2 estimation. PyCO2SYS can estimate pCO2 uncertainty by propagating the TA uncertainty (Humphreys et al., 2022). The uncertainty of estimated TA leads to ±11% uncertainty in pCO2 estimation, however there was no significant difference in the river's CO_2 state over 32 years, as detailed in the uncertainty analysis in **Appendix B, Section B3**.

FCO_2 (mmol C m^{-2} d^{-1}) between the water and the atmosphere was calculated using Fick's law, using the CO_2 transfer velocity (kCO_2, m d^{-1}) and the air-water CO_2 gradient (mmol m^{-3}) (Eq. 1). We obtained kCO_2 (Eq. 2) using Schmidt number (Sc) at given water temperature (Eq. 3) scaling from the gas transfer velocity k_{600} (m d^{-1}) (Raymond et al., 2012a). The k_{600} was calculated by multiplying river depth with K_{600}, an output of *streamMetabolizer*. The k600 estimates from the StreamMetabolizer model were selected for FCO_2 calculations to ensure consistency with the NEP calculations.

$$FCO_2 = k_{CO_2} \times (CO_{2\,water} - CO_{2\,air}) \quad \text{Eq. 1}$$

$$k_{CO_2} = depth \times K_{600} / \left(600/Sc_{CO_2}\right)^{-0.5} \quad \text{Eq. 2}$$

$$\mathrm{Sc}_{\mathrm{CO}_2} = 1911.1 - (118.1 \times T) + (3.45 \times T^2) - (0.0413 \times T^3) \quad \text{Eq. 3}$$

196 $CO_{2,water}$ is aqueous CO_2 (mmol m^{-3}) estimated by pyCO2SYS, and $CO_{2,air}$ is CO_2 in equilibrium with
197 the atmosphere using global monthly atmospheric CO_2 from 1990–2021 from National Oceanic and
198 Atmospheric Administration Global Monitoring Laboratory (https://gml.noaa.gov/ccgg). K_{600} is the gas
199 exchange rate coefficient normalized to a Schmidt number of 600 (d^{-1}) from streamMetabolizer, Sc_{CO2}
200 is the Schmidt number for CO_2 (unitless), T is the water temperature in degrees Celsius (°C). We used
201 Henry's law to convert pCO_2 in µatm into CO_2 in mmol m^{-3} using temperature-dependent solubility
202 constants.

203 *2.3.3. Categorizing NEP-FCO_2 states by autotrophic/heterotrophic and source/sink states*

204 We categorized the river into four trophic-flux states (or "trophlux" states) based on daily NEP and
205 FCO_2. Following Odum (1956), if NEP is positive (GPP > ER), the river is autotrophic, while if NEP is
206 negative (GPP < ER), the river is heterotrophic. Likewise, if FCO_2 is positive, the river is a CO_2 source,
207 while if FCO_2 is negative, the river is a CO_2 sink, relative to the atmosphere. The river could thus be in
208 four possible trophlux states: 1) autotrophic-sink, 2) autotrophic-source, 3) heterotrophic-sink, and 4)
209 heterotrophic-source. The autotrophic-sink and heterotrophic-source states imply that NEP and FCO_2
210 vectors are moving CO_2 in the same direction, into water column biomass or out of the water column,
211 respectively (Bogard & Del Giorgio, 2016). The remaining two states imply opposite directions between
212 NEP and FCO_2. The autotrophic-source state implies that although there is a net conversion of CO_2 into
213 biomass, there is a surplus of water column CO_2 relative to autotrophic needs, leading to continued
214 positive FCO_2. The heterotrophic-sink state implies that despite the net conversion of biomass into water
215 column CO_2, there is still a CO_2 undersaturation relative to the atmosphere, likely due to prior
216 autotrophic uptake. We expect the heterotrophic-sink state to be a temporary occurrence, reflecting
217 temporal lags within the carbonate system buffering capacity during the short transition between
218 autotrophic and heterotrophic states. Recent work using this dataset has provided strong evidence for
219 this mechanism, showing that these events are temporary and typically follow periods of intense
220 autotrophic activity (Diamond et al., 2025). A more detailed discussion of methodological
221 considerations for this state is provided in **Appendix B, Section B4**.

Conventionally, the aquatic metabolism contribution to river CO_2 emissions (i.e., the internal CO_2 source) is calculated as $-NEP/FCO_2$ in the heterotrophic-source state (Bernal et al., 2022; Hotchkiss et al., 2015; Kirk & Cohen, 2023).

2.4. Change points and long-term trend analysis

To test our hypothesis that FCO_2 would vary as a function of ecosystem state and metabolism shifts in the Loire River, we compared change points in FCO_2 with previously estimated change points in ecosystem regime(ca. 2005) and metabolic regime (ca. 2012) (Diamond et al., 2022; Minaudo et al., 2015). We used the *ruptures* Python package (Truong et al., 2020) with a five-year window interval to ensure that identified changes were sustained beyond year-to-year variation. The change point detection was also applied to the daily NEP and related variables (pH, alkalinity, pCO_2, k600, GPP, and ER). We also conducted change point detection on the seasonal decomposed time series of daily FCO_2 and NEP. This decomposition, performed using the *statsmodels* Python package (Seabold & Perktold, 2010), separates a time series into trend, seasonal, and residual components, allowing us to specifically identify change points in the characteristics of the seasonal cycle (e.g., amplitude changes) independently of the long-term trend (**Appendix C, Section C1)**. To quantitatively assess differences between change point periods, we performed non-parametric Kruskal-Wallis tests followed by post-hoc Mann-Whitney U tests (**Appendix C, Section C2**).

We further estimated long-term trends of FCO_2 and NEP as functions of hydroclimatic conditions (discharge, water temperature) in each trophlux state by using the Mann-Kendall test (*pyMannKendall* Python package) (Hussain & Mahmud, 2019).

2.5. Seasonal hysteresis of NEP and FCO_2 in response to discharge changes

To test the influence of discharge on CO_2 emissions, we evaluated the hysteresis of mean daily FCO_2 and NEP against mean daily discharge across the periods delineated by the change point analysis. We predicted that for the same discharge, FCO_2 would exhibit a range of magnitudes depending on the season but that this range would decrease systematically as a function of decreasing phytoplankton coverage in the Loire River. We evaluated the hysteresis loops by the direction of hysteresis (clockwise

248 or counterclockwise) and the magnitude (i.e., difference of FCO_2 at the same discharge but in the rising
249 and falling flow stage). We anticipated that the shift to a macrophyte-dominated regime, with potentially
250 more stable GPP across flow conditions, might lead to a reduction in the magnitude (i.e., a "flattening")
251 of these hysteresis loops for FCO2 and NEP. We additionally calculated hysteresis magnitude for –NEP,
252 external source contribution (FCO_2 + NEP), and –NEP/FCO_2 at the mean discharge (300 $m^3 s^{-1}$, Table
253 2) during the rising (autumn) and falling stage (spring).

254 **3. Results**

255 **3.1. Daily, seasonal, inter-annual FCO_2 emissions and NEP contribution for 32 years**

256 FCO_2 and NEP exhibited strong daily, seasonal, and inter-annual variations (Figure 1). The pronounced
257 seasonal variability drove successive transitions among different trophlux states. Typically, the river
258 would shift from being heterotrophic and a CO_2 source in winter, towards becoming more autotrophic
259 in spring and potentially a CO_2 sink in summer during low flows, before returning to heterotrophic
260 source conditions in autumn with rising flows. This general seasonal pattern, involving changes in both
261 NEP (autotrophic/heterotrophic) and FCO_2 (sink/source), recurred each year, though its specific timing
262 and intensity varied (Figure 1c). The corresponding hydro-climatic context, including mean annual
263 discharge for each year, is provided in the Supplementary Information (Figure S3) for a detailed
264 comparison.

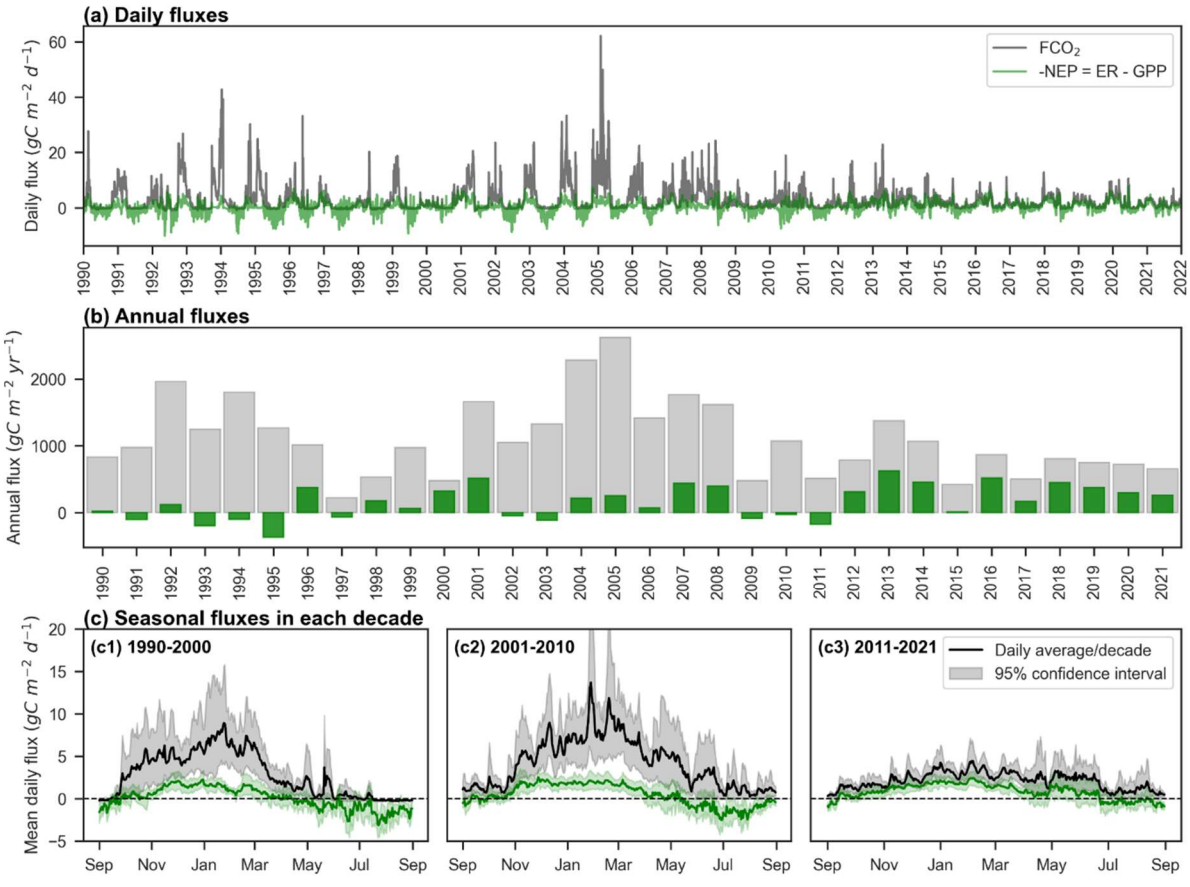

Figure 1. Evolution of FCO_2 and –NEP during 1990-2021. (a) Daily values (g C m^{-2} d^{-1}), (b) Cumulative annual fluxes (calendar year, g C m^{-2} y^{-1}), (c) Seasonal fluxes during hydrological year in each decade 1990-2000, 2001-2010, 2011-2021. In Figure 1c, the solid line and shaded area are the average and the 95% confidence interval of the daily fluxes each decade, calculated by 10 daily fluxes in the same day-year.

The daily average FCO_2 was 3 g C m^{-2} d^{-1}, with high peaks reaching 20 - 60 gC m^{-2} d^{-1} during high flow in winter (1000–2000 m^3 s^{-1}) and low peaks with negative FCO_2 of -0.8 gC m^{-2} d^{-1} during the low flow in summer (<150 m^3 s^{-1}) (Figure 1). The daily NEP was -0.45 gC m^{-2} d^{-1}, with average peaks from -4.0 gC m^{-2} d^{-1} in winter to 3.6 gC m^{-2} d^{-1} in summer (Figure 1a).

Cumulative annual FCO_2 ranged from 221 to 2633 g C m^{-2} y^{-1} and NEP from -383 to 584 g C m^{-2} yr^{-1}. Notably, there were 10 years when the Loire River was net autotrophic (Figure 1b, green bars), mainly in 1990-2000. Even during these years, the Loire River was a net source of CO_2 to the atmosphere (Figure 1b, grey bars). The contribution of external CO_2 sources (FCO_2 + NEP) ranged from 800–2400 g C m^{-2} y^{-1} in 1990–2010. However, the contribution of external CO_2 sources has significantly decreased to ca. 400 g C m^{-2} y^{-1} since 2011 (Figure 1b).

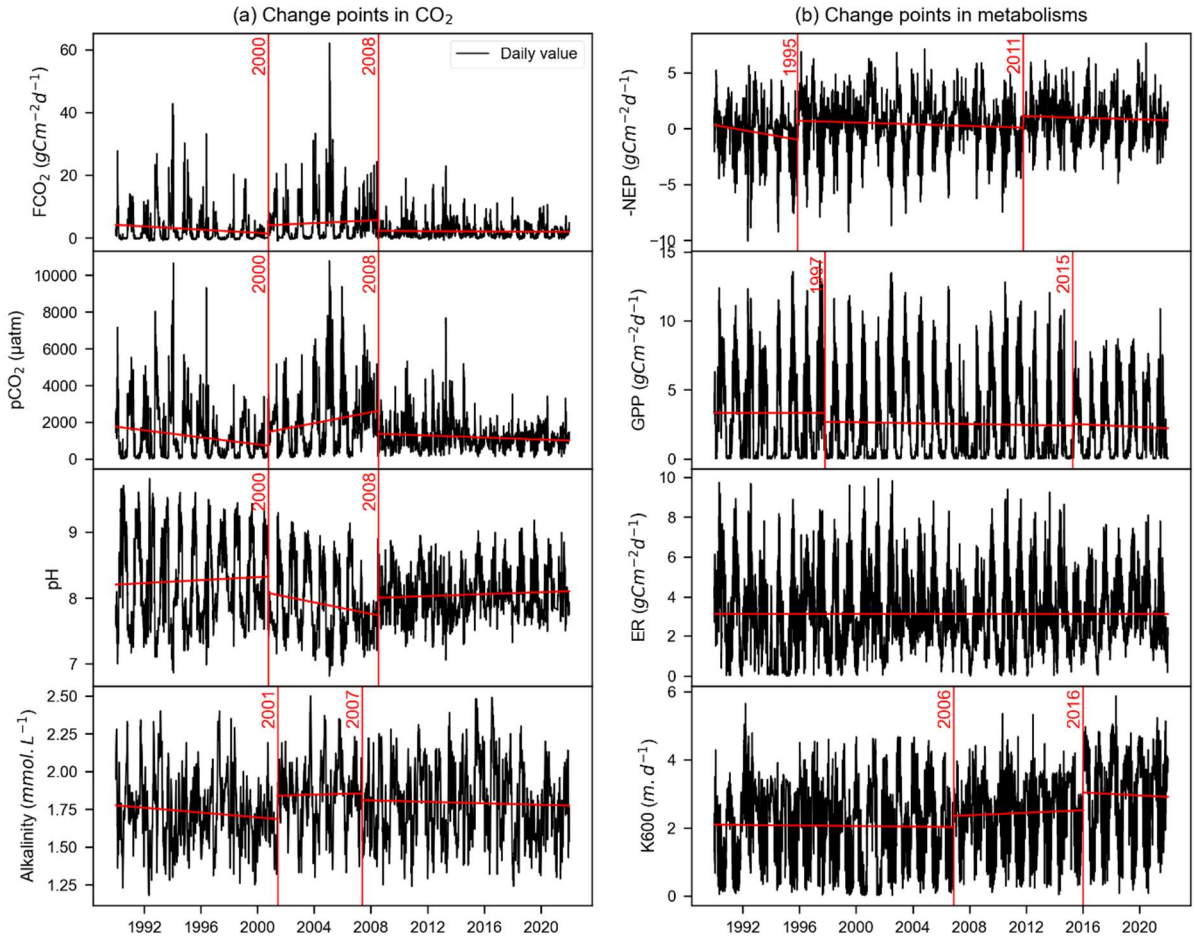

Figure 2. Change point detection in the daily time series of (a) FCO_2, pCO_2, pH, alkalinity and (b) –NEP, K600, GPP, ER during 1990-2021. The vertical red lines indicate the year of the change point.

The change point analysis on daily time series detected that the FCO_2 experienced two change points in 2000 and 2008 (Figure 2a), while the change points of –NEP were detected in 1995 and 2011 (Figure 2b). While change points in –NEP described a gradual increase, change points in FCO_2 indicated more abrupt fluctuations, with abnormal decreases in 2000 and 2008. The daily time series of pCO_2, pH, and alkalinity had similar change points to FCO_2. The change points of –NEP were mainly dependent on GPP, while there was no significant change in the ER time series (Figure 2b). In addition, the seasonal decomposition analysis detected the same change point in 2008 for the seasonal amplitude in both FCO_2 and NEP, indicating a significant decrease in the seasonal variations (Figure C1).

The periods of change in both FCO_2 and NEP spanned roughly three decades: (i) 1990–2000, (ii) 2001–2010, and (iii) 2011–2021. These time frames were selected based on changepoint analysis, which identified shifts in FCO_2 around 2000 and 2008, in NEP around 1995 and 2011, and GPP around 1997

and 2015 (Figure 2). Despite some discrepancies in the exact timing of these changepoints between FCO_2 and NEP, grouping the data by decades allowed for a coherent comparison of long-term trends in ecosystem behavior. These periods corresponded to distinct phases in river metabolism and CO_2 emissions: (i) high primary productivity (cumulative annual GPP= 1113 ± 225 g C m^{-2} y^{-1}, ER= 1136 ± 241 g C m^{-2} y^{-1}) and low CO_2 emission (FCO_2 = 1031 ± 531 g C m^{-2} y^{-1}) ; (ii) reduced primary productivity (GPP= 973 ± 292 g C m^{-2} y^{-1}, ER= 1136 ± 128 g C m^{-2} y^{-1}) and high CO_2 emission (FCO_2 = 1534 ± 620 g C m^{-2} y^{-1}), and (iii) low primary productivity (GPP= 867± 212 gC m^{-2} y^{-1}, ER= 1167 ± 163 g C m^{-2} y^{-1}) and low CO_2 emission (FCO_2 = 773 ± 272 g C m^{-2} y^{-1}).

3.2. Occurrence and contribution of trophlux states to CO_2 emissions

At the seasonal time scale, the Loire River varied among trophlux states, with the heterotrophic-source state predominating. The source state occurred the least (64% of time) in the first decade delineated by change points (1990–2000) and occurred the most (92% of time) in the most recent decade (2011–2021). Likewise, the heterotrophic state occurred at a minimum of 54% and a maximum of 67% of time during those decades, respectively. The joint occurrence of the heterotrophic-source state thus ranged from 47.3 ± 9.4% in 1990-2000 to 66.8 ± 11.3% in 2011-2021 (Table 1), coinciding with low water temperature and high discharge (Figure C2). This state contributed more than 90% of the total annual CO_2 emissions. Within this heterotrophic-source state, the contribution of internal sources (–NEP/FCO_2) to total CO_2 emissions varied across the decades: it was 37 ± 27% in 1990-2000, 28 ± 9% in 2001-2010, and increased to 57 ± 10% in 2011-2021 (Table 1). This implies that external CO_2 sources accounted for the remaining proportion in each period.

The remaining three trophlux states (autotrophic-source, autotrophic-sink, and heterotrophic-sink) had a combined net impact of less than 10% on total FCO_2 despite their regular occurrence (e.g., up to 50% of time) during the 1990-2000 decade. The autotrophic-sink state, driven by high GPP, typically occurred for 1–3 months during the summer growing season, coinciding with the highest water temperatures and the lowest discharge (Table 1). The autotrophic-sink reduced annual FCO_2 by -3.0 ± 4.2% during 1990–2000 and by -0.4 ± 0.3% in 2011–2021. In spring and autumn, the Loire River was regularly in an autotrophic state (17% to 28% of time) but remained a CO_2 source, presumably attributed

to external CO_2 sources. This autotrophic-source state contributed 8.2–9.2% to annual FCO_2 across years. The heterotrophic-sink state occurred rarely (1–7% of time) and had a small influence on the annual FCO_2 budget (reducing it by 0.1% to 0.8% across the decades). This state typically occurred as relatively short events of 1–14 days from June to August during the transition from autotrophic-sink state or heterotrophic-source state.

Table 1. Summary of the occurrence, fluxes, and related hydroclimatic conditions of each trophlux state in three decades, 1990-2021. The values within the table are depicted as the mean annual value ± standard deviation, calculated for each decade (N=10 or 11).

Variable	Period	CO_2 source		CO_2 sink		All states
		Heterotrophic	Autotrophic	Heterotrophic	Autotrophic	
Occurrence (% of days)	1990-2000	47.3 ± 9.4	16.7 ± 9.2	7.3 ± 5.4	28.7 ± 7.0	100
	2001-2010	61.2 ± 12.7	25.3 ± 11.2	1.7 ± 1.1	15.5 ± 9.0	100
	2011-2021	65.8 ± 11.3	26.2 ± 8.6	1.1 ± 1.5	7.3 ± 5.7	100
FCO_2 budget (% of annual flux by each state)	1990-2000	94.6 ± 13.8	9.2 ± 11.4	-0.8 ± 1.4	-3.0 ± 4.2	100
	2001-2010	92.4 ± 11.3	8.2 ± 11.2	-0.1 ± 0.0	-0.6 ± 0.5	100
	2011-2021	91.8 ± 5.6	8.7 ± 5.8	-0.1 ± 0.2	-0.4 ± 0.3	100
–NEP ($gC\ m^{-2}\ y^{-1}$)	1990-2000	277 ± 158	-54 ± 46	25.5 ± 28.0	-225 ± 97	23 ± 222
	2001-2010	376 ± 127	-111 ± 83	3.8 ± 3.0	-131 ± 100	162 ± 234
	2011-2021	417 ± 173	-82 ± 48	2.0 ± 2.4	-36 ± 35	300 ± 232
FCO_2 ($gC\ m^{-2}\ y^{-1}$)	1990-2000	954 ± 514	102 ± 148	-4.4 ± 4.5	-21 ± 12	1031 ± 531
	2001-2010	1453 ± 666	88 ± 104	-0.6 ± 0.8	-7.8 ± 5.4	1534 ± 620
	2011-2021	717 ± 274	59 ± 28	-0.9 ± 1.8	-2.6 ± 2.1	773 ± 272
External CO_2 ($gC\ m^{-2}\ y^{-1}$)	1990-2000	677 ± 477	157 ± 92	-29 ± 32	204 ± 93	1008 ± 551
	2001-2010	1077 ± 595	199 ± 172	-4 ± 1	123 ± 95	1372 ± 528
	2011-2021	299 ± 140	140 ± 55	-2 ± 3	34 ± 31	472 ± 129
–NEP/FCO_2 (%)	1990-2000	37 ± 27	*	*	**	5 ± 29
	2001-2010	28 ± 9	*	*	**	7 ± 15
	2011-2021	57 ± 10	*	*	**	34 ± 27
Temperature (°C)	1990-2000	8 ± 4	12 ± 4	18 ± 3	20 ± 3	13 ± 6
	2001-2010	10 ± 5	18 ± 5	18 ± 7	21 ± 3	13 ± 7
	2011-2021	11 ± 5	18 ± 5	10 ± 9	21 ± 3	14 ± 6
Discharge ($m^3\ s^{-1}$)	1990-2000	454 ± 326	276 ± 225	115 ± 60	111 ± 56	301 ± 290
	2001-2010	436 ± 323	160 ± 110	137 ± 69	115 ± 59	323 ± 296
	2011-2021	362 ± 278	120 ± 87	205 ± 136	80 ± 63	277 ± 259

*** Not applicable. In these cases, the –NEP/FCO_2 ratio does not represent a simple contribution of internal respiration to CO_2 evasion and is therefore not reported. The mass balance for these states is presented in Figure 5.**

**** Not Applicable. Internal metabolism consumes both external CO_2 and the CO_2 supplied from the atmosphere through the gas exchange at the air-water interface.**

The external CO_2 ($gC\ m^{-2}\ y^{-1}$) = FCO_2 + NEP

3.3. The inter-annual trend of FCO_2 depending on trophlux states

The occurrence of heterotrophic-source and autotrophic-sink and their contribution to FCO_2 gradually changed from 1990 to 2021 (Figure 3). The occurrence of the heterotrophic-source state increased from 140 days in 1990 to 250 days in 2021 (Figure 3a). However, the annual flux of –NEP within this state remained relatively stable (Figure 3b), while FCO_2 decreased with an average rate of 0.16 g C m^2 d^{-1} per year, resulting in a 62% reduction of FCO_2 in the heterotrophic-source state over the 32 years (Figure 3d). The annual decline in FCO_2 was uncorrelated (R^2 = 0.09) with the increase in annual water temperature (+5.7 °C/32 years), but it was positively correlated (R^2 = 0.36) with the decrease in annual discharge (-13%/32 years) (Table D1). Since the annual –NEP remained stable and FCO_2 decreased, the ratio of –NEP/FCO_2 thus increased from 20–40% in the 1990s to 60-75% in recent years, +1.25% per year (Figure 3f). There were some abnormal increases of –NEP/FCO_2 observed in 1995–2000, with the ratio reaching 100% in 1997 and 90% in 1996 and 2000. These peaks were associated with a significant drop in FCO_2 (Figure 3d) and, thus, in external CO_2 sources (Figure 3b).

The autotrophic-sink state occurrence decreased from 140 days in 1990–2000 to 30 days in recent years (Figure 3a), following a reduction in +NEP from about 2 to 1.5 gC m^{-2} d^{-1} (-25%/32 years), corresponding to -0.015 g C m^2 d^{-1} per year (Figure 3b). In this state, annual discharge and temperature did not show significant changes ($p > 0.05$) (Figure 3c, e). The decrease in +NEP was not significantly correlated with either annual discharge (R^2 = 0.03) or annual temperature (R^2 = 0.00) (Table D2).

Regarding the other two trophlux states, the autotrophic-source state showed a significant increasing trend in occurrence, similar to the heterotrophic-source state (Figure 3a). This state was also associated with increasing annual temperatures and decreasing annual discharge over time (Figure 3c,e). However, unlike the heterotrophic-source state, there was no significant long-term trend in FCO_2. In contrast, the heterotrophic-sink state existed rarely over the study period and showed no significant long-term trends due to its very infrequent occurrence.

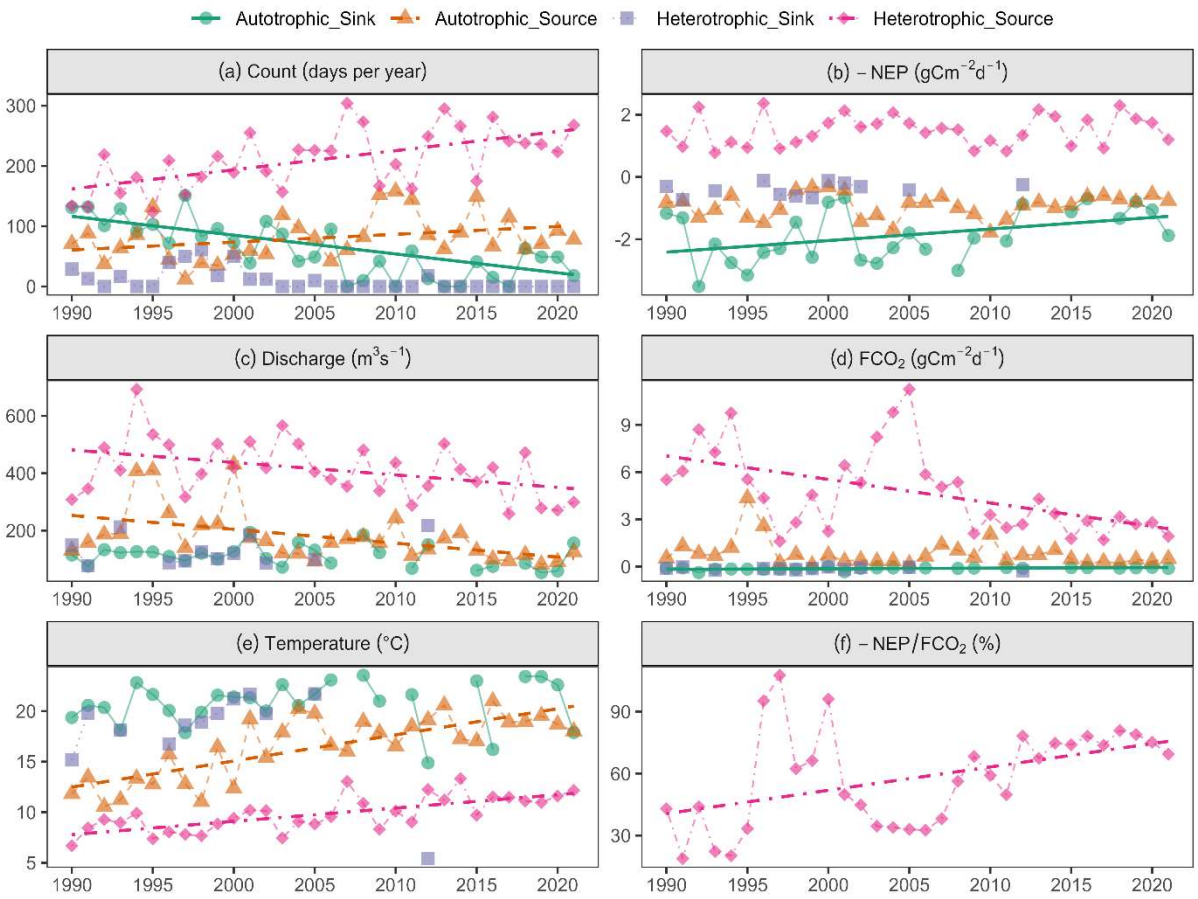

Figure 3. Long-term trends over 32 years of CO_2 fluxes, aquatic metabolism contribution, and hydroclimatic conditions on each trophlux state: a) occurrence per year, b) annual aquatic metabolism flux (–NEP), c) annual discharge, d) annual FCO_2, e) annual water temperature, f) –NEP/FCO_2. The points depicted on the graph were the annual averages. The regression lines were the Theil-Sen slopes with significant trends (p-value < 0.05).

3.4. Seasonal hysteresis of NEP and FCO_2 in relation to discharge

FCO_2 and NEP exhibited a similar clockwise hysteresis pattern in response to seasonal variations of discharge, i.e., higher fluxes in the rising discharge stage compared to the falling stage (Figure 4). Typically, hysteresis cycles started with FCO_2 minima and NEP maxima in July and August (mean discharge <150 m^3 s^{-1}, mean temperature 23 °C), with opposite peaks in January and February (mean discharge >500 m^3 s^{-1}, mean temperature 5 °C) (Figure 4a). As river discharge gradually increased from summer to winter, the river transitioned from an autotrophic to a heterotrophic state and from CO_2 sink to source. Subsequently, but along a different trajectory, the river shifted back to an autotrophic state during the spring-summer falling discharge stage (150–300 m^3 s^{-1}). During this time, however, the river continued to act as a CO_2 source, lasting two to three months (April–June) before returning to the FCO_2

minimum again in summer. The contribution of external CO_2 sources (FCO_2 + NEP) also exhibited a clockwise hysteresis loop with discharge, with higher external contributions during the rising limb (autumn/winter) and lower contributions during the falling limb (spring) at equivalent discharge rates, generally mirroring the patterns observed for FCO_2 and –NEP (Figure 4, bottom row).

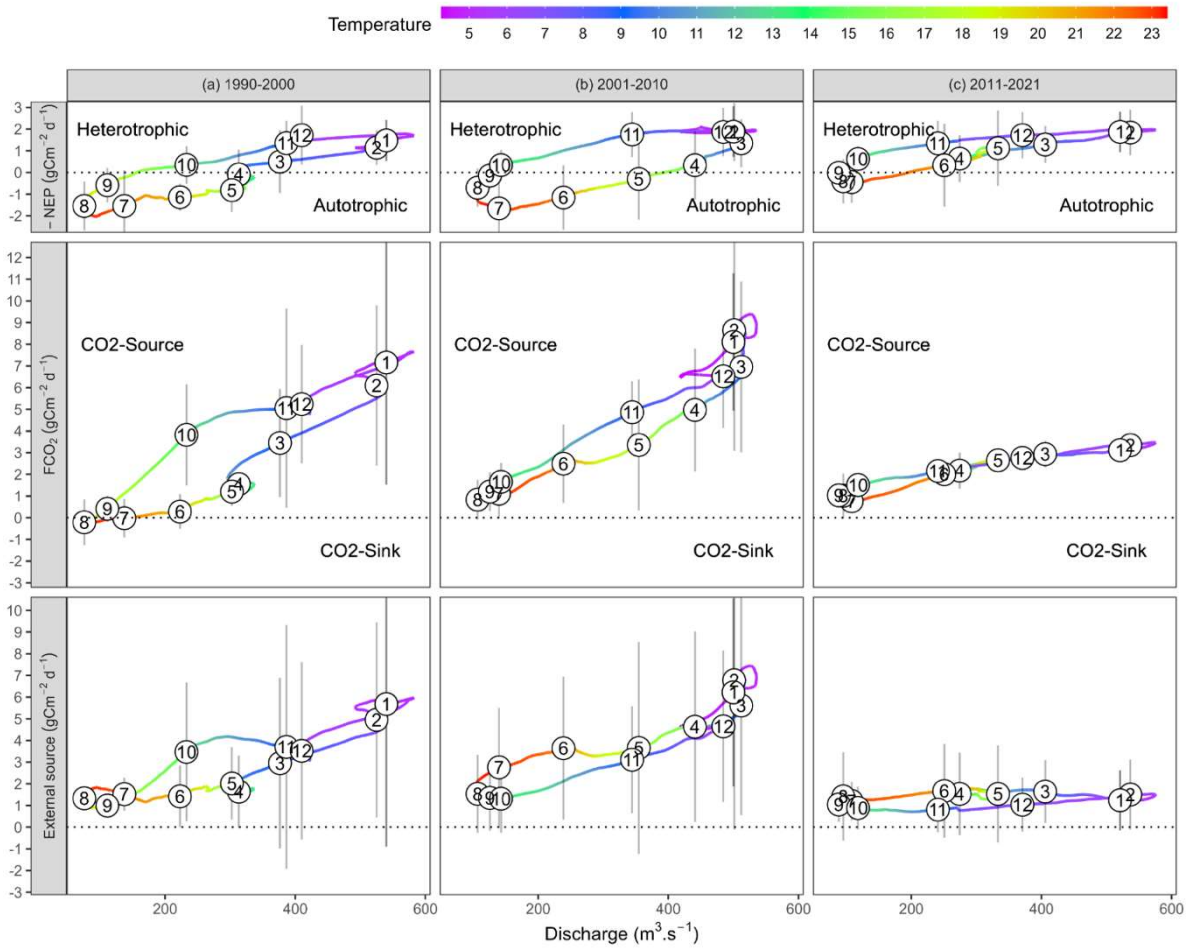

Figure 4. Hysteresis loops of –NEP, FCO_2, and external sources (FCO_2 + NEP) during the hydrological cycle in each decade 1990-2000, 2001-2010, and 2011-2021. The color lines are the daily average fluxes in each decade. The circle shape with numbers is the monthly average and standard deviation fluxes in each decade.

The discharge trajectories of –NEP, FCO_2, and external sources varied across the three decades delineated by the change point analysis. In three decades, all hysteresis loops exhibited positive relationships with discharge, except the external CO_2 sources in 2011–2021. FCO_2 hysteresis magnitude at 300 $m^3 s^{-1}$ (autumn–spring) decreased from 3.2 g C $m^{-2} d^{-1}$ in 1990–2000 to -0.09 g C $m^{-2} d^{-1}$ in 2011–2021. The near-zero FCO_2 hysteresis magnitude at 300 $m^3 s^{-1}$ in 2011–2021 (Table 2) indicates that FCO_2 values at this discharge were very similar during both the rising (autumn) and falling (spring)

limbs of the hydrograph. This reduction in the hysteresis loop area suggests that the relationship between FCO_2 and discharge became less dependent on the seasonal progression of the hydrograph in recent years, making FCO_2 at a given moderate discharge more predictable regardless of season. Likewise, the magnitude of –NEP hysteresis at 300 $m^3 s^{-1}$ was weakest in recent years (0.68 g C $m^{-2} d^{-1}$), but unlike FCO_2, it exhibited a peak (2.12 g C $m^{-2} d^{-1}$) in 2001–2010 (Table 2).

The internal source contribution of FCO_2 (–NEP/FCO_2) at 300 $m^3 s^{-1}$ between spring and autumn had contrasting ratios, with a positive CO_2 contribution in autumn (14 – 34%) but a negative contribution in spring (-26%, i.e., CO_2 consumption) in 1990-2000 and 2001-2010 (Table 2). In 2011-2021, internal source contributions of FCO_2 in autumn and spring were both positive, 64% and 34%, respectively.

Table 2. The mean ± standard deviation fluxes of daily –NEP, FCO_2, external CO_2, and –NEP/FCO_2 in spring and autumn at the mean river discharge of 300 ± 30 ($m^3 s^{-1}$).

	Flux*	1990–2000	2001–2010	2011–2021
River metabolism (g C $m^{-2} d^{-1}$)	$-NEP_{300}$ spring	-0.28 ± 0.41	-0.69 ± 0.11	0.83 ± 0.18
	$-NEP_{300}$ autumn	0.66 ± 0.15	1.43 ± 0.13	1.5 ± 0.06
	$-NEP_{300}$ hysteresis	0.94 ± 0.43	2.12 ± 0.17	0.68 ± 0.18
Total CO_2 fluxes (g C $m^{-2} d^{-1}$)	$FCO_{2\ 300}$ spring	1.55 ± 0.44	2.65 ± 0.15	2.42 ± 0.12
	$FCO_{2\ 300}$ autumn	4.77 ± 0.14	4.15 ± 0.25	2.34 ± 0.08
	$FCO_{2\ 300}$ hysteresis	3.22 ± 0.47	1.5 ± 0.29	-0.09 ± 0.14
External CO_2 flux (g C $m^{-2} d^{-1}$)	($FCO_{2\ 300}$+ NEP_{300}) spring	1.83 ± 0.2	3.34 ± 0.05	1.59 ± 0.14
	($FCO_{2\ 300}$+NEP_{300}) autumn	4.12 ± 0.05	2.72 ± 0.12	0.83 ± 0.05
	($FCO_{2\ 300}$+NEP_{300}) hysteresis	2.29 ± 0.2*	-0.62 ± 0.13**	-0.76 ± 0.15
–NEP/FCO_2 (%)	–NEP/$FCO_{2\ 300}$ spring	-26 ± 33%	-26 ± 5%	34 ± 6%
	–NEP/$FCO_{2\ 300}$ autumn	14 ± 3%	34 ± 1%	64 ± 1%
	–NEP/$FCO_{2\ 300}$ hysteresis	40 ± 34%	61 ± 5%	30 ± 6%

***** The hysteresis flux is equal to the difference of flux in autumn and spring, i.e., 2.29 = 4.12–1.83, where the 300 subscript refers to the fact that these measurements are averages from mean discharge at 300 $m^3 s^{-1}$.
****** Negative hysteresis flux indicates lower flux in autumn (rising waters stage), i.e., -0.62 = 2.72–3.34

4. Discussion

Our data analysis reveals important long-term changes in carbon fluxes of the Loire River. Re-oligotrophication led to an increase in the contribution of internal source of FCO_2, supporting our hypothesis but for reasons that ran counter to our predictions. Indeed, under oligotrophic conditions and macrophyte dominance, –NEP/FCO_2 increased by fourfold overall under the heterotrophic-source state,

with –NEP contributing up to 75% of FCO_2 at the monitoring station during the last decade (Figure 3). However, this change was largely due to decreases in total FCO_2 rather than an increase in the magnitude of –NEP. Instead, decreases in FCO_2 appeared to be due to an approximate halving of external CO_2 sources (Figure 5). Still, the timing of FCO_2 shifts, as detected by our change point analysis (ca. 2000 and 2010), broadly corresponded to our predictions based on previous studies (i.e., 2005 for trophic state change and 2012 for metabolism change), suggesting similar drivers of external and internal CO_2. Finally, we observed clear support for our prediction of weaker discharge controls on FCO_2 and –NEP/FCO_2 based on hysteresis analysis. However, this appeared to be most strongly due to a weakened discharge-external CO_2 source link rather than a weakened discharge-internal CO_2 source link.

4.1. Trophlux states and their contribution to CO_2 emissions

Large river systems function predominately as a source of CO_2 to the atmosphere (Battin et al., 2023; Butman & Raymond, 2011; Cole et al., 2007; Raymond et al., 2013; Abril and Borges 2019), and CO_2 sink states are rarely observed, even in large eutrophic rivers (Raymond et al., 1997). However, our unique dataset revealed the commonality of CO_2 sink behavior in the Loire River and further highlighted the seasonal transitions among all four possible trophlux states and how these transitions varied annually and across decades (Figure 1, Figure 4). This finding challenges the conventional understanding of large rivers as persistent CO_2 sources and demonstrates how ecosystem metabolism can fundamentally alter carbon cycling patterns. The frequency of CO_2 sink conditions in the Loire River reveals an important but often overlooked aspect of river carbon budgets that may be significant for other large temperate systems undergoing similar environmental changes. The transitions among these trophlux states are influenced by seasonal climatic drivers (temperature, solar radiation, discharge patterns, which themselves are subject to long-term climate change) and broader environmental changes like nutrient loading (e.g., re-oligotrophication) or external factors such as groundwater, making such long-term analyses critical for systems undergoing similar pressures.

We found that, regardless of the long-term trophic regime, the heterotrophic/source state was the most prevalent (47–66% of time), while the autotrophic-source state occurred for approximately a quarter of the year (17–26% of time) (Figure 5). By contrast, the mean annual occurrence of the autotrophic-sink

state depended strongly on the trophic conditions of the river, decreasing from 28.7 ± 7.0% of days in the eutrophic 1990-2000 period to 7.3 ± 5.7% in the oligotrophic 2011-2021 period (Table 1). This shift in trophlux state dominance reflects the ecosystem's response to re-oligotrophication (Diamond et al., 2022). Reduced nutrient availability, particularly phosphorus, directly restrained GPP more substantially than ER because ER is supported by both autochthonous organic matter (linked to GPP) and allochthonous inputs from the catchment. The declining prevalence of autotrophic-sink conditions indicates that the river's capacity to sequester atmospheric CO_2 has diminished with the transition from phytoplankton to macrophyte dominance. This demonstrates how long-term changes in trophic status can fundamentally alter carbon dynamics beyond simple changes in productivity rates.

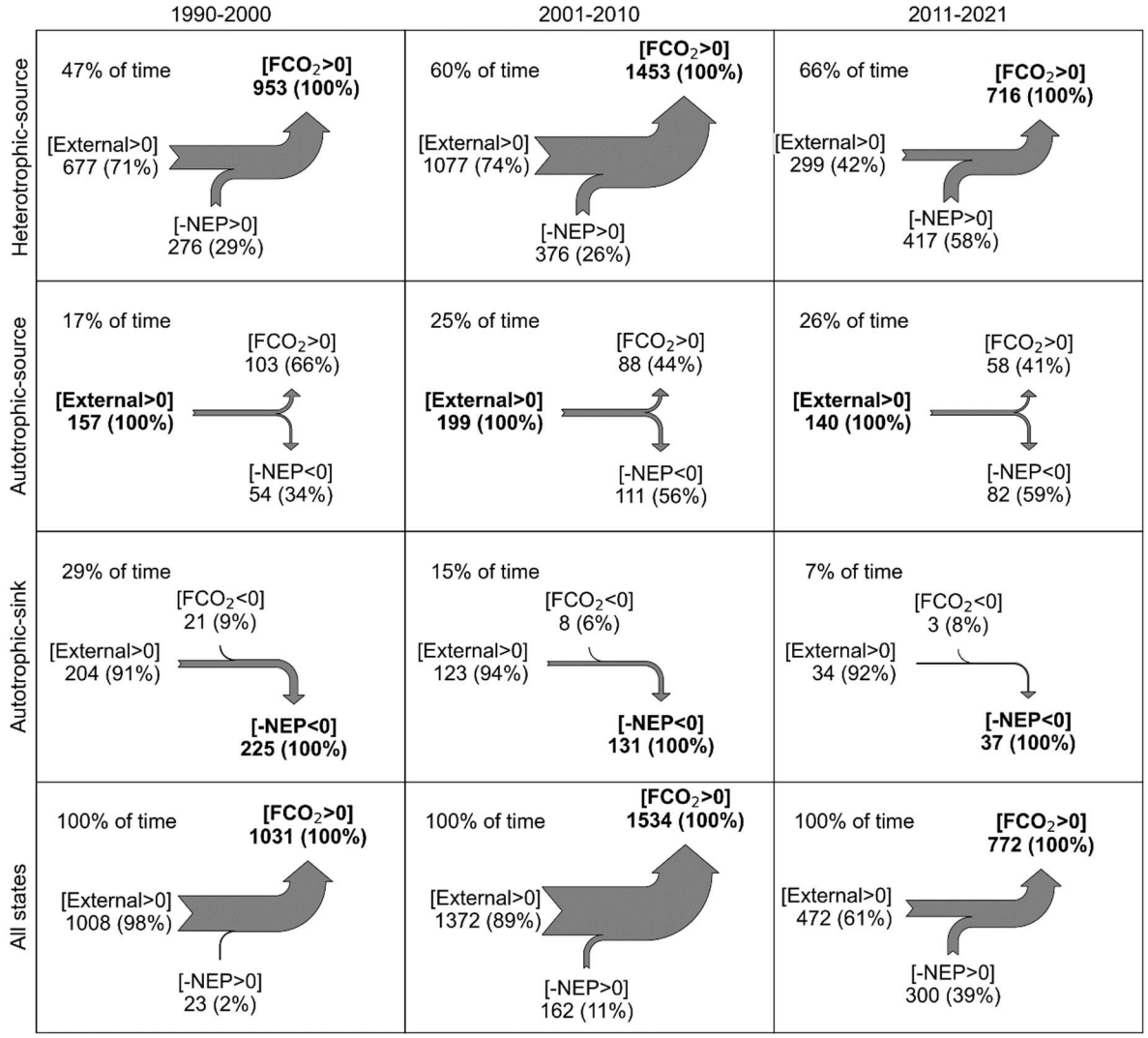

Figure 5. Annual CO_2 budget in three main trophlux states in 1990–2000, 2001–2010, and 2011–2021. All flux values are expressed in units of gC m^{-2} y^{-1}. The notation [FCO_2 > 0] denotes CO_2 emissions from rivers to the atmosphere, whereas [FCO_2 < 0] signifies CO_2 ingassing. The percentages in

parentheses represent the proportion of each flux component, with the percentage calculated relative to the maximum flux component (shown in black bold).

4.2. Changes in CO_2 sources in relation to hydrology and re-oligotrophication

This work provides a significant long-term perspective to our understanding of the contribution of internal and external sources to FCO_2 in large rivers. Despite this decades-old research question (Cole et al., 2001), the capacity to quantify the relative strength of these two fluxes is relatively recent (Bernal et al., 2022; Hotchkiss et al., 2015; Kirk & Cohen, 2023), and data in mid-sized and large rivers are still limited. Utilizing a dataset comprising five rivers with mean discharge >100 m^3 s^{-1}, Hotchkiss et al. (2015) estimated an NEP of -0.51 to -1.01 g C m^{-2} d^{-1} and –NEP/FCO_2 of 25% to 54%. More recently, Solano et al. (2023) highlighted the vast range of this contribution, with values spanning from less than 10% to over 100%. Our results in the Loire River, which show strong seasonal variability in this metric, align with this broader context. This reinforces that within a single large river system, the contribution of internal metabolism to FCO_2 can be highly dynamic, covering much of the spectrum reported across diverse global systems.

While the magnitude of discharge is a known control on CO_2 dynamics, our results highlight that the seasonal timing and the rising or falling limb of the hydrograph are equally crucial for determining CO_2 fluxes and sources, due to hysteresis effects. Depending on the season, our results caution that measurements at the same discharge may yield contrasting estimates of the internal source contribution (Table 2, Figure 4). This difference was mainly explained by the difference in NEP magnitude and not by differences in FCO_2. For example, at the same mean discharge, NEP in autumn during the rising stage was more negative, and the river was more heterotrophic than in spring during the falling stage. This difference was only partly explained by differences in daily temperature between the two seasons (R^2=0.29, Figure D1). First autumn floods are known to mobilize labile organic matter in temperate rivers, whose drying river beds in summer accumulate plant litter from riparian vegetation (Coynel et al., 2005; Etcheber et al., 2007). In the Middle Loire, the emergence of large, fertile riverbanks during the summer dry season may lead to organic matter deposition that is easily remobilized in autumn. Indeed, Minaudo et al. (2015) observed that the heterotrophy in the Middle Loire in autumn was strongly stimulated by a larger availability of biodegradable organic matter compared to spring. Such a seasonal

hydrology-driven variability in river heterotrophy and associated CO_2 dynamics was also recently observed by Young et al. (2025) in the Upper Clark Fork River, USA. They reported pronounced seasonal variation in FCO_2 primarily linked to snowmelt-driven hydrological events mobilizing terrestrial carbon sources, reinforcing our observations that river CO_2 dynamics are strongly shaped by seasonal hydrological connectivity and terrestrial organic matter inputs.

Notably, Figure 4 reveals decadal changes in the magnitude of these hysteresis patterns. The FCO2 hysteresis magnitude at 300 $m^3 s^{-1}$ decreased dramatically from 3.2 g C $m^{-2} d^{-1}$ in 1990–2000 to -0.09 gC $m^{-2} d^{-1}$ in 2011–2021, indicating a weakening discharge-FCO_2 relationship in recent years. Similarly, external source hysteresis (bottom row, Figure 4) has flattened considerably in 2011-2021, suggesting diminished influence of terrestrial carbon inputs on seasonal CO_2 dynamics. As these insights would have been invisible without a high-frequency long-term dataset (Figure 1), we, therefore, encourage future efforts to capture seasonality and varying discharges in the measurement campaigns.

During the 1990–2000 decade, the Loire River acted as a CO_2 sink for almost half the years due to high rates of GPP. The occurrence of this state has gradually declined over the three decades (Table 1), highlighting an important environmental trade-off where improved water quality from re-oligotrophication has diminished the river's capacity to act as a CO_2 sink. In 1990–2000, the biogeochemical dynamics of the Loire River during the summer months coincided with long water residence times, shallow waters, low discharge, high water temperature, and high eutrophication (>200 µg chlorophyll-a L^{-1}) (Moatar et al., 1999, 2001). These conditions were similar to eutrophic lakes, which regularly act as CO_2 sinks (Bogard & Del Giorgio, 2016; He et al., 2022). In addition, autotrophy can exert a stronger control on CO_2 dynamics in larger rivers compared to small streams. This is due to factors such as increased light penetration across wider channels supporting higher areal GPP, and a larger water volume where internal metabolic signals may be less rapidly overwhelmed by the proportional influence of external CO_2 inputs from groundwater or riparian zones (Hotchkiss et al., 2015). Our data show that in the Loire, the long-term shift from phytoplankton to macrophyte-dominance in 2005 has resulted in a decrease in NEP and greater heterotrophy. Diamond et al. (2021) showed that the changes in stream metabolism in the Loire River in 2010–2012 were related to the shift

of other state variables in 2005 (turbidity, nutrient concentrations, Corbicula fluminea densities, and chlorophyll-a), suggesting a decade lag for metabolism shift. Moreover, while annual water temperature increased (+0.18°C per decade, +5.7°C over 32 years) and annual river discharge decreased (-4% per decade, -13% over 32 years) (Figure 3, Table D1), these hydroclimatic trends did not show a direct, strong correlation with the timing or magnitude of these decadal metabolic shifts (Figure D2), suggesting that their manifestation on the magnitude of NEP is insignificant.

4.3. Long-term changes in the external CO_2 source

Contrary to our expectations, we observed a decreasing trend of FCO_2 attributable to an over 50% reduction in external CO_2 sources in the Loire River. At first glance, this may appear to be due to overall reductions in discharge and the magnitude of lateral CO_2 transport from groundwater and wetlands to the river (Abril & Borges, 2019). While our data show a modest long-term decline in total river discharge (~13% over 32 years), this alone is insufficient to explain the large reduction in external CO_2 inputs (Figures D1 & D2). Besides, the linkage between external CO_2 and river discharge is more consistent with the seasonal variation (Figure 4, Figure D1) rather than the inter-annual variation (Figure D2). In addition, while the discharge can explain ca. 37-48% of the decay in FCO_2, it only explains ca. 19-26% of the variation in external CO_2 source magnitude (Figures D1 and D2). Similarly, in a forested sandy watershed, Deirmendjian et al. (2018) reported that the export of CO_2 flux from groundwater to the stream was independent of stream discharge and relatively constant seasonally. This can be explained by the fact that higher discharge periods in these systems are associated with low dissolved CO_2 groundwater concentrations and vice-versa. Still, to explain the >500 g C m^{-2} y^{-1} reduction in external CO_2 between 2001-2010 and 2011-2021, it seems clear that some reduction in groundwater CO_2 is occurring. This decrease in external inputs must be driven by either a decrease in the volume of contributing groundwater or a decrease in the CO_2 concentration of that groundwater, or a combination of both.

In regions with carbonate bedrock, weathering of carbonate minerals can significantly contribute to the CO_2 flux through the production of alkalinity (Vihermaa et al., 2014). Although this weathering reaction does not directly release CO_2, it provides bicarbonate ions (HCO_3^-), which can equilibrate with CO_2 and

526 subsequently degas under certain conditions, influencing the CO_2 flux observed in groundwater and
527 rivers. Additionally, the transfer of CO_2 to groundwater depends on the spatiotemporal connections
528 between zones of maximal soil respiration and their intersection with the water table (Tsypin &
529 Macpherson, 2012). If the water table remains disconnected from the topsoil where respiration is
530 strongest, the transfer of soil CO_2 to groundwater becomes limited. Trend analysis of the groundwater
531 table in France over the past 30 years shows low-frequency variations of multi-annual (~7 years) and
532 decadal (~17 years) cycles in groundwater level (Baulon et al., 2022). Further evidence from a
533 representative local borehole at Montifault (20 km from our site) shows a clearly decreasing trend in the
534 piezometric level since 2003 (Appendix D, Figure D3). This regional decrease in groundwater levels
535 supports a reduction in groundwater discharge to the river.

536 To further explore the potential drivers behind the inferred long-term decrease in external CO_2 inputs,
537 we analyzed available data of pH and TA during 1990-2021 from several groundwater monitoring
538 stations situated in aquifers hydraulically connected to our study site. This analysis revealed a long-term
539 increasing trend in groundwater pH, particularly after 2008, while groundwater TA remained relatively
540 stable (Figure D4). At stable alkalinity, an increase in pH directly corresponds to a decrease in pCO_2.
541 This inferred decline in groundwater pCO_2 provides a strong, complementary mechanism explaining the
542 observed reduction in external CO_2 inputs to the river. Given the relative stability of in-river TA over
543 the study period (Figure 2), it is likely that these shifts in the carbonate system are driven by changes in
544 CO_2 supply rather than major changes in catchment-scale weathering rates. In addition, a study at a site
545 located 20 km downstream from our study area in the Val d'Orléans fluviokarst aquifer reported that
546 dissolved inorganic carbon flux from groundwater has decreased by about 20% along with the decrease
547 of groundwater level between 2000 and 2020 (Binet et al., 2022). Binet et al. (2022) also assessed that
548 there was no significant change in the carbonate weathering rate at this aquifer, which is similar to the
549 relatively stable alkalinity at the Loire River (Figure 2). Together, the evidence for both reduced
550 groundwater discharge and lower groundwater pCO_2 provides a robust explanation for the observed
551 multidecadal decline in external CO_2 sources to the Loire River.

5. Conclusions

In the middle Loire River, three main trophlux states alternately occur in the hydrological year cycle, predominated by the heterotrophic-source state. The heterotrophic-source state contributes more than 90% of annual CO_2 emissions, with an average of 40% from internal contribution (–NEP). Besides, in the 1990s, the autotrophic-sink state was still common; however, this state has gradually disappeared in recent years with the decline of phytoplankton, replaced by the dominance of macrophytes. Our analysis of seasonal hysteresis of NEP and CO_2 fluxes in relation to discharge indicates stronger heterotrophy in autumn during rising waters than in spring during the falling waters, and this is partly explained by river temperature but more likely due to the remobilization of organic matter in floodplains and secondary channels during the first floods.

We report a strong long-term decrease in CO_2 fluxes (-62% over the 32 years) and an increase in the contribution of heterotrophy (–NEP) to this CO_2 outgassing flux. While our study infers changes in external CO_2 sources, a full understanding of carbon transfer at the groundwater-river interface requires more DIC data from groundwaters and riparian zones (Deirmendjian & Abril, 2018; Duvert et al., 2018). Future work should focus on obtaining such data to quantify these fluxes better. We also suggest that developing approaches to extrapolate findings from such detailed site studies across diverse river networks, integrating them with spatial hydrological and ecological data, will be key to better understanding and predicting how global changes will influence the balance between internal and external CO_2 production at broader scales, ultimately refining estimates of the role of rivers in the global carbon budget.

Appendix A: Dataset integrity and validation

This appendix provides detailed information on the data acquisition, quality assurance/control (QA/QC) framework, and processing procedures used to generate the 32-year high-frequency dataset.

A1. Data acquisition and QA/QC framework

The dataset combines high-frequency continuous monitoring data from Électricité de France (EDF) with lower-frequency grab sample data from both EDF and the Loire-Brittany Water Agency (AELB).

The continuous measurement system of EDF is a floating platform with a temperature sensor and sensors for pH (range 0–14 pH unit), DO (range 0–20 mg L^{-1}), and conductivity (range 0–1000 µS cm^{-1})

(Campbell l ®). The surface water at 20 cm depth is pumped (ca. 0.5 L s^{-1}) through the system and measurements are recorded every 5 seconds, with average values saved every hour. It should be noted that data was collected both upstream and downstream of the nuclear power plant, with the upstream station located at the entrance of the dam and the downstream station located approximately 2-5km downstream of the dam. The data used for data analysis in this study was from the upstream station because of its data completeness. Grab sampling data was collected by EDF and Loire-Brittany Water Agency (AELB), including pH, conductivity, and TA in 1990-2021, with frequency ranging from daily to monthly. Grab sampling data exists only upstream of the nuclear power plant. While AELB provided data for the period of 1990 to 2003 for these parameters, EDF supplied data from 2007 to 2021.

EDF's environmental monitoring operates under mandatory oversight from ASN (Autorité de Sûreté Nucléaire), France's nuclear safety authority, with QA/QC protocols documented for two main periods. Prior to 2008, measurements were made with membrane sensors and validated using a multi-level quality control methodology that included routine calibrations and automated checks (Moatar et al., 2001), achieving an accuracy of approximately ±0.3 pH units and ±8% for DO. In 2008, the sensor technology was upgraded to optical sensors, and since 2009, all procedures have complied with ISO 17025:2005 standards, requiring documented calibration with certified reference standards and regular external audits.

We cross-validate the pH data from EDF with independent Water Agency grab samples (www.naiades.eaufrance.fr). The cross-validation confirms measurement continuity across the sensor transition, showing improved post-2008 agreement (pH residuals: -0.17±0.35 to -0.10±0.32 pH units) while preserving statistically significant long-term trends (**Figure A1**). Post-2008 optical sensors indicate fewer differences with the grab samples, but both continuous sensor data from EDF and grab sample data from the water agency are well consistent with the long-term trend. This demonstrates that the sensor upgrade enhanced data quality rather than creating systematic artifacts, with the step change in 2008 contributing to but not solely explaining the multidecadal trends.

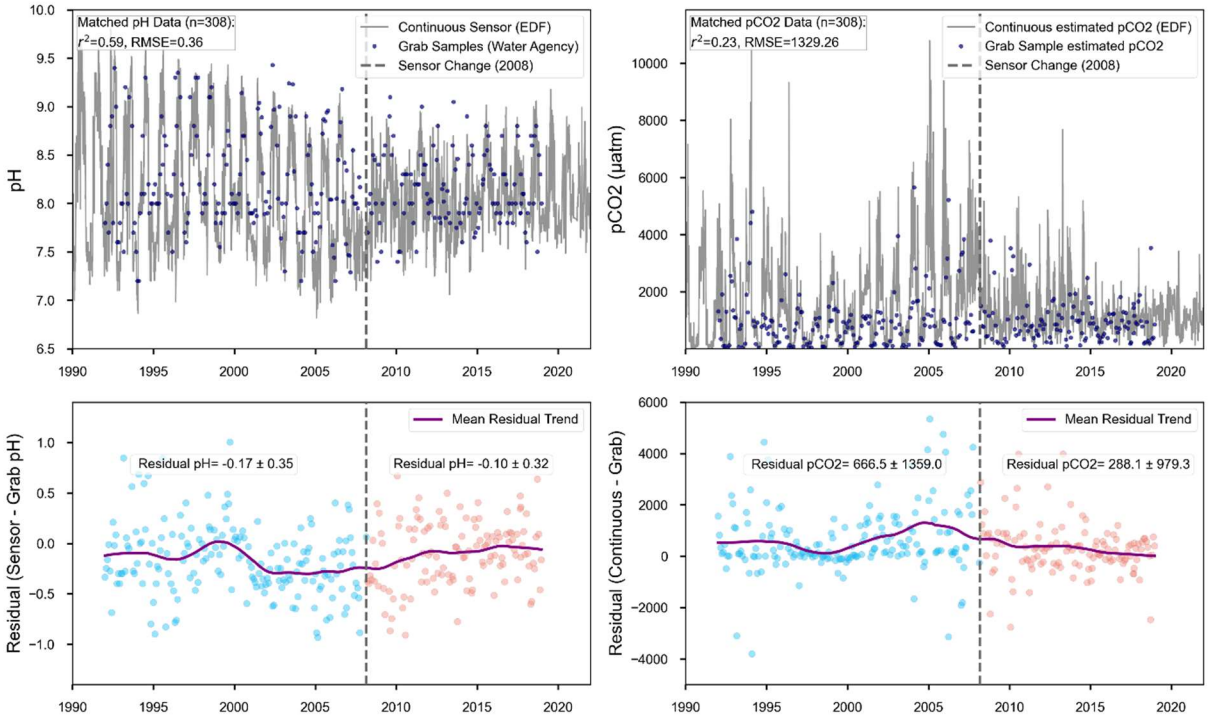

605

606 **Figure A1.** Comparison of continuous sensor (EDF) vs. independent grab samples from the water
607 agency for pH and estimated pCO_2 in 1990-2021. Bottom panels show residuals (Sensor - Grab) with
608 points colored pre/post sensor change in 2008, a LOWESS trend, and mean residual ± SD.

609 **A2. Data Processing and Reconstruction**

610 **Data Cleaning:** Although the sensors for pH and DO measurements were periodically calibrated by
611 EDF, the dataset still exhibited a notable number of anomalous values prior to 2008, which prompted
612 the implementation of comprehensive data control procedures. These procedures addressed sensor drift
613 and outlier removal, which were proposed by (Moatar et al., 2001). Data cleaning was conducted for the
614 hourly pH and dissolved oxygen data in this study, while the daily conductivity was carried out by EDF,
615 which was heavily based on visual inspection. Hourly temperature and alkalinity data from grab
616 sampling were only checked through a range check to eliminate unrealistic values, but there was minimal
617 significant removal of this data.

618 The following steps were carried out for the data cleaning and correction for hourly pH. Firstly,
619 performing the rules-based anomaly detection and correction as a first pass at quality control, including
620 range check (pH ranges from 6 to 10 in Loire River), data persistence check (pH relatively constant in
621 few days), significant change check (jump or drop within few hours), calibration and drift event
622 detection check. This step was performed automatically with the support of *pyhydroqc,* a Python
623 package for automating aquatic sensor data processing (A. S. Jones et al., 2022). Secondly, error
624 detection was manually inspected by comparing values between upstream and downstream, together
625 with daily discharge. This step used the interactive plot with the support of *plotly* package to check the

errors that were identified in previous steps. The use of daily discharge was to eliminate false detection of abnormal data, especially in the case of high discharge, where there are often sudden changes in pH and conductivity. There was 10.6% data (about 3 years of data) that was assessed as anomalous and was discarded. Finally, missing data will be completed based on several cases. Linear interpolation was applied for missing data within 6 hours (2.3% of data). Linear interpolation between upstream and downstream stations was applied for missing either upstream or downstream (7.5% of data). Linear interpolation between adjacent stations was applied when missing data in both upstream and downstream at the Dampierre station, but existed in adjacent stations (0.5% data). The remaining missing data was then filled based on the seasonal Kalman smoother, which estimates the missing values while considering the seasonal patterns and annual trend (*tsmoothie* package) (0.3% data).

The data cleaning procedure was similar for hourly DO. We first removed physically impossible values and then applied a low-pass filter to remove instrument noise in the DO signal. We then removed values that exceeded plausible hourly changes in DO (e.g., a leap from 10 to 15 mg L^{-1}) using 95% confidence intervals for hourly changes on a monthly basis as our cutoff. We finally used visual inspection to flag data of questionable validity and corrected for linear drift and anomalous drops or jumps in DO data. We then filled all remaining missing values with a seasonal Kalman filter (3% data). The data cleaning and correction for hourly DO were detailed by Diamond et al. (2025).

Alkalinity Reconstruction: As daily TA data were not available for the entire 32-year period, a continuous daily TA time series was reconstructed from the continuous daily conductivity data.

To reconstruct daily alkalinity from conductivity, we employed the *IterativeImputer* function with *BayesianRidge* estimator (i.e., regularized linear regression) by using *scikit-learn*, a Python package. The *BayesianRidge* estimator filled the missing daily alkalinity by iteratively modeling the linear relationship between daily conductivity and available alkalinity data, while regularization accounts for potential changes in their relationship over 32 years. This process begins by estimating data for the period with the fewest missing data, then continues iteratively until the imputed values converge, meaning subsequent iterations produce minimal changes in the estimates. This iterative process allows the imputer to adapt to underlying trends and shifts in the data. Besides, to verify the stability of the relationship between alkalinity and conductivity, we performed linear regressions on a 4-year period of 32 years dataset, which revealed quite similar slopes across all periods except 1990-1993 **(Figure A2**).

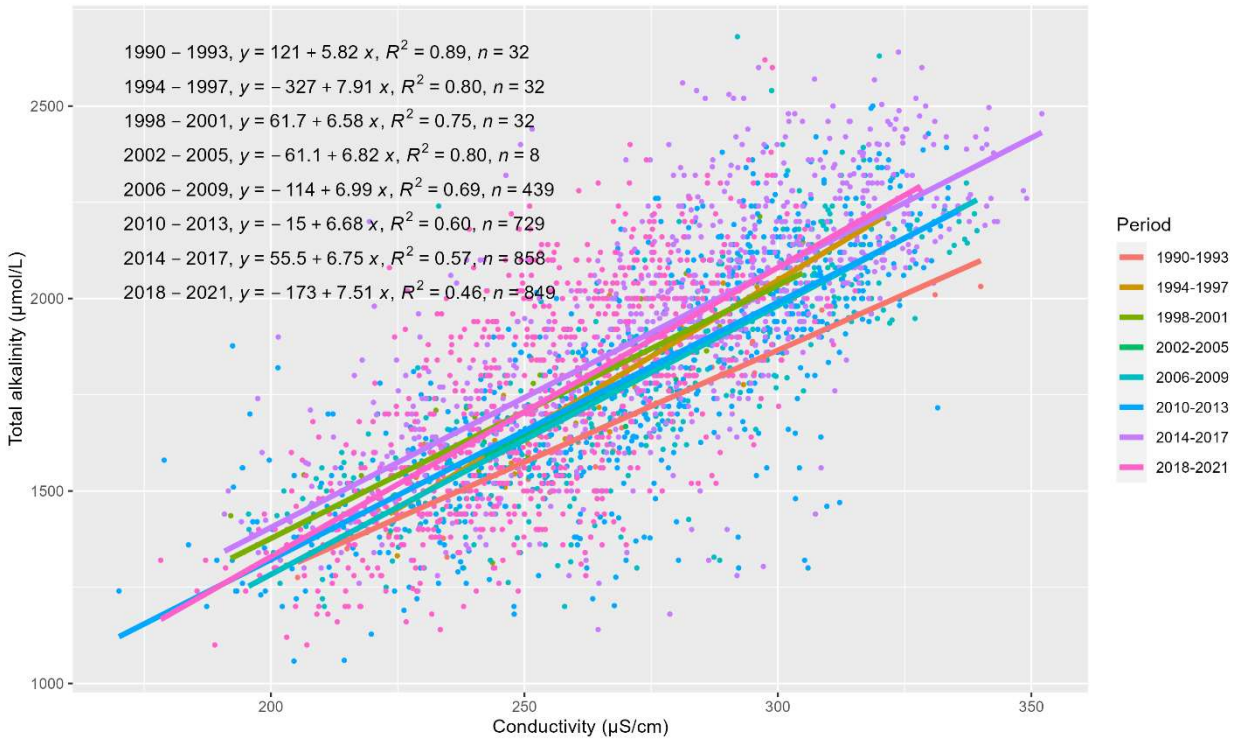

Figure A2. Relationship between measured total alkalinity and continuous measured conductivity in the Loire River.

Appendix B: Model Validation and Uncertainty

This appendix details the methods for handling model outputs, validates key model parameters, and assesses the impact of uncertainty on the final conclusions.

B1. Handling of Metabolism Model Outputs

The streamMetabolizer model can occasionally produce physically unrealistic values, such as negative GPP or positive ER. This issue typically arises when diel variations in dissolved oxygen (DO) are weak—meaning the DO levels are similar between day and night—making it difficult for the model to accurately separate the contributions of GPP and ER (Appling et al., 2018). When the diel DO signal is minimal, the GPP is likely close to zero, which can lead to the model estimating a negative median GPP value. Consequently, it is common practice to set these negative GPP estimates to zero (Blaszczak et al., 2019). In our study, rather than forcing these estimates to zero, we replaced unrealistic estimates with the 75th percentile of the modeled posterior distribution for that day. This approach avoids artificially setting values to zero while still acknowledging that the true value is likely small.

In general, this correction did not substantially alter the annual GPP or ER calculations. Replacing negative GPP with the 75th percentile increased annual GPP by an average of 1.3% (ranging from 0.1% to 5.3%), while setting negative GPP to zero resulted in a smaller increase, ranging from 0.04% to 3.4% (**Figure B1).** Similarly, the annual ER calculations across different treatments for unrealistic ER values

show no significant differences, with an average flux variation of around 1%, except in 1995, where the difference reaches 15% **(Figure B2).**

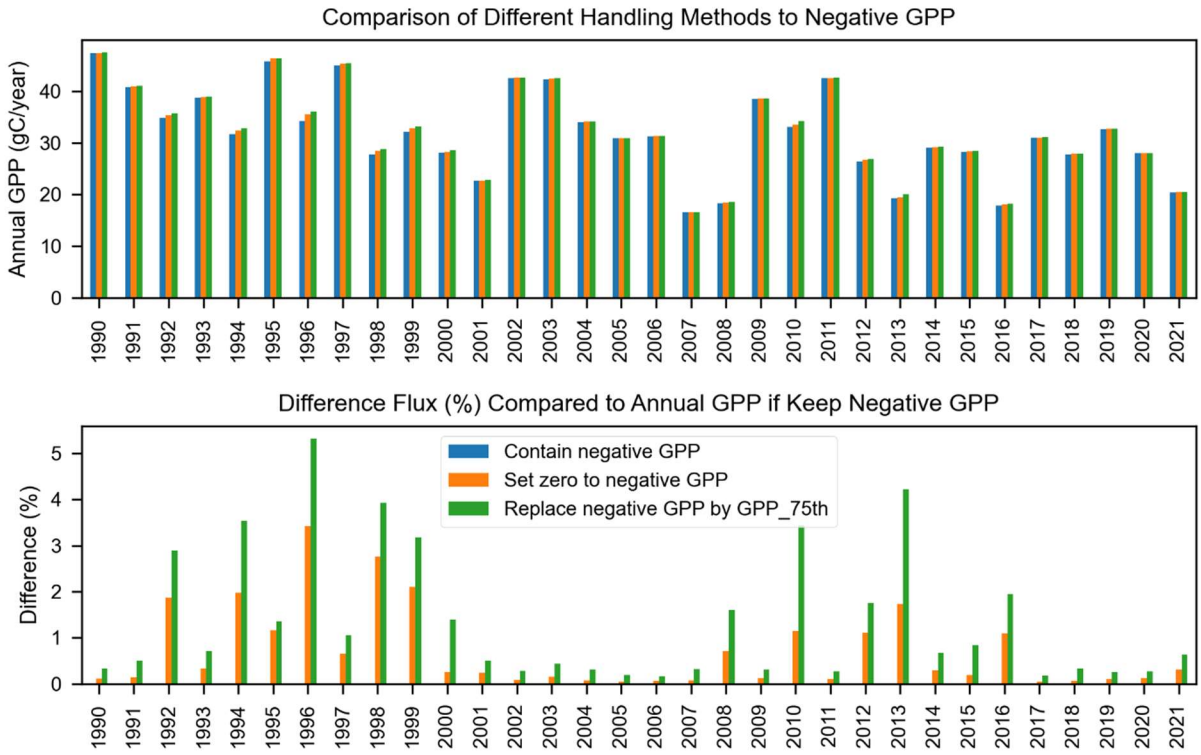

Figure B1. Comparison of annual GPP estimates based on different approaches for handling negative GPP values: retaining negative GPP, setting negative GPP to zero, and replacing negative GPP with the 75th percentile of estimated GPP from the *streamMetabolizer* model.

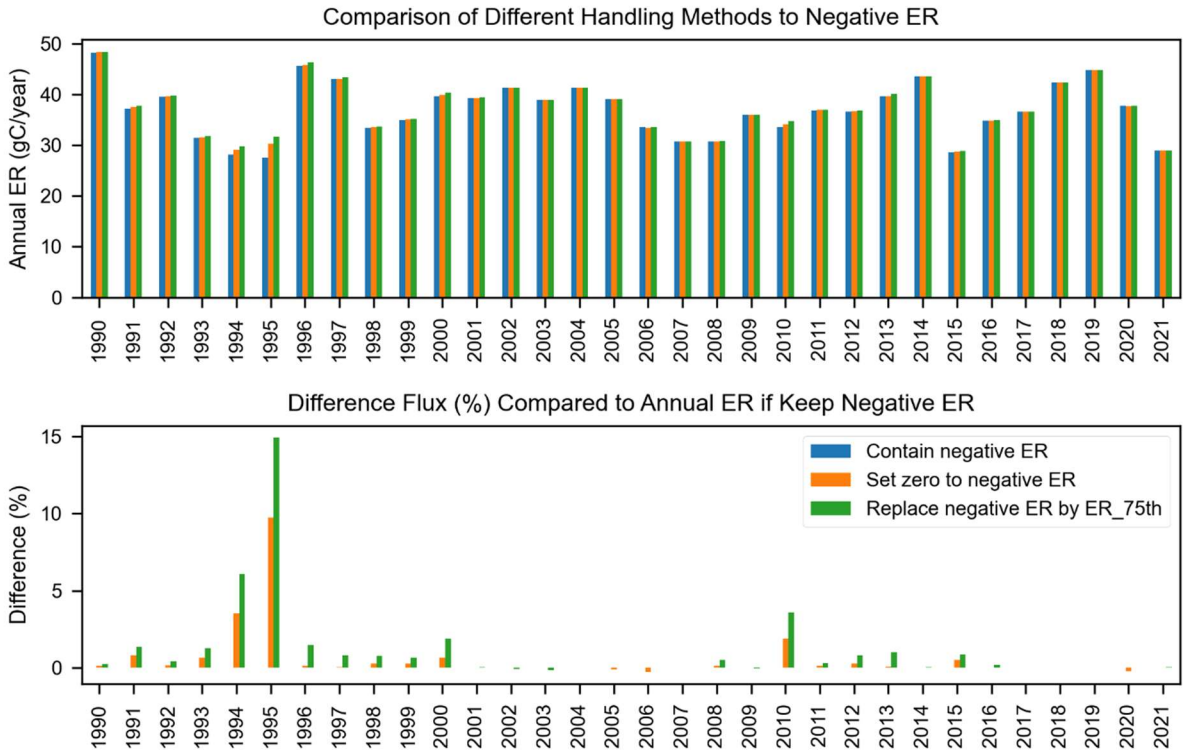

Figure B2. Comparison of annual ER estimates based on different approaches for handling negative ER values: retaining negative ER, setting negative ER to zero, and replacing negative ER with the 75th percentile of estimated ER from the *streamMetabolizer* model.

B2. Validation of the Gas exchange coefficient (k600)

The k600 values estimated by the StreamMetabolizer model were compared with the seven k600 values calculated from seven fitted equations proposed by Raymond et al. (2012b) for streams and small rivers. Both k600 estimates exhibited similar seasonal fluctuations, with the lowest values occurring in summer and the highest in winter (Figure **B3**). The comparison revealed that the mean absolute percentage error (MAPE) between the StreamMetabolizer estimates and the mean k600 from the seven fitted equations ranged from 36% to 62%. Specifically, the Raymond et al. (2012) k600 estimates tended to be higher in summer (low discharge) and lower in winter (high discharge) compared to those estimated by the StreamMetabolizer model (Figure **B4**). Such discrepancies can arise because streamMetabolizer co-estimates K600 with GPP and ER by fitting observed DO dynamics, making its estimate sensitive to the strength of the biological signal, whereas empirical equations rely solely on hydraulic proxies for turbulence. At high flow (winter), streamMetabolizer may underestimate k600 because the strong turbulence and deep water can weaken the biological signal (i.e., the daily change in dissolved oxygen), which the model relies on for its estimations. The Raymond et al. (2012) hydraulic equations, by contrast, are driven by high velocity and are less sensitive to this biological signal dampening. At low flow (summer), streamMetabolizer may estimate a higher k600 because the biological signal is very

strong and clear in the shallow, warm, and productive water. The model may attribute a larger portion of the observed oxygen change to gas exchange to best fit the data.

However, the k600 values derived from StreamMetabolizer fall within the same order of magnitude as those from the seven fitted equations (Figure **B3**). To maintain internal consistency between the metabolic and FCO_2 calculations, the k600 estimates from streamMetabolizer were used for all subsequent flux calculations.

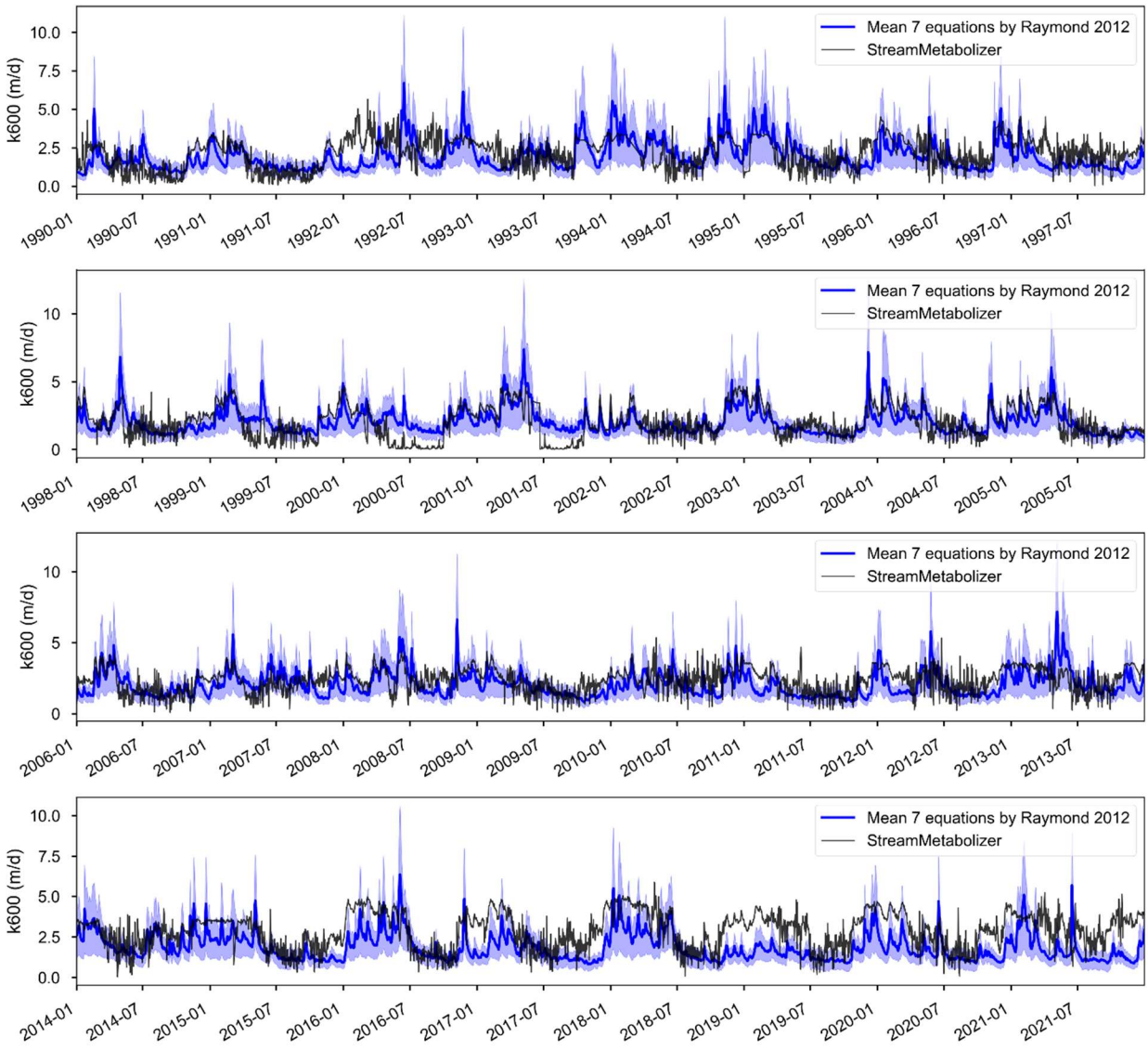

Figure B3. Comparison of the gas exchange coefficient (k600) estimated by streamMetabolizer (black line) with the mean and range (blue shaded area) of values derived from seven empirical equations from Raymond et al. (2012b).

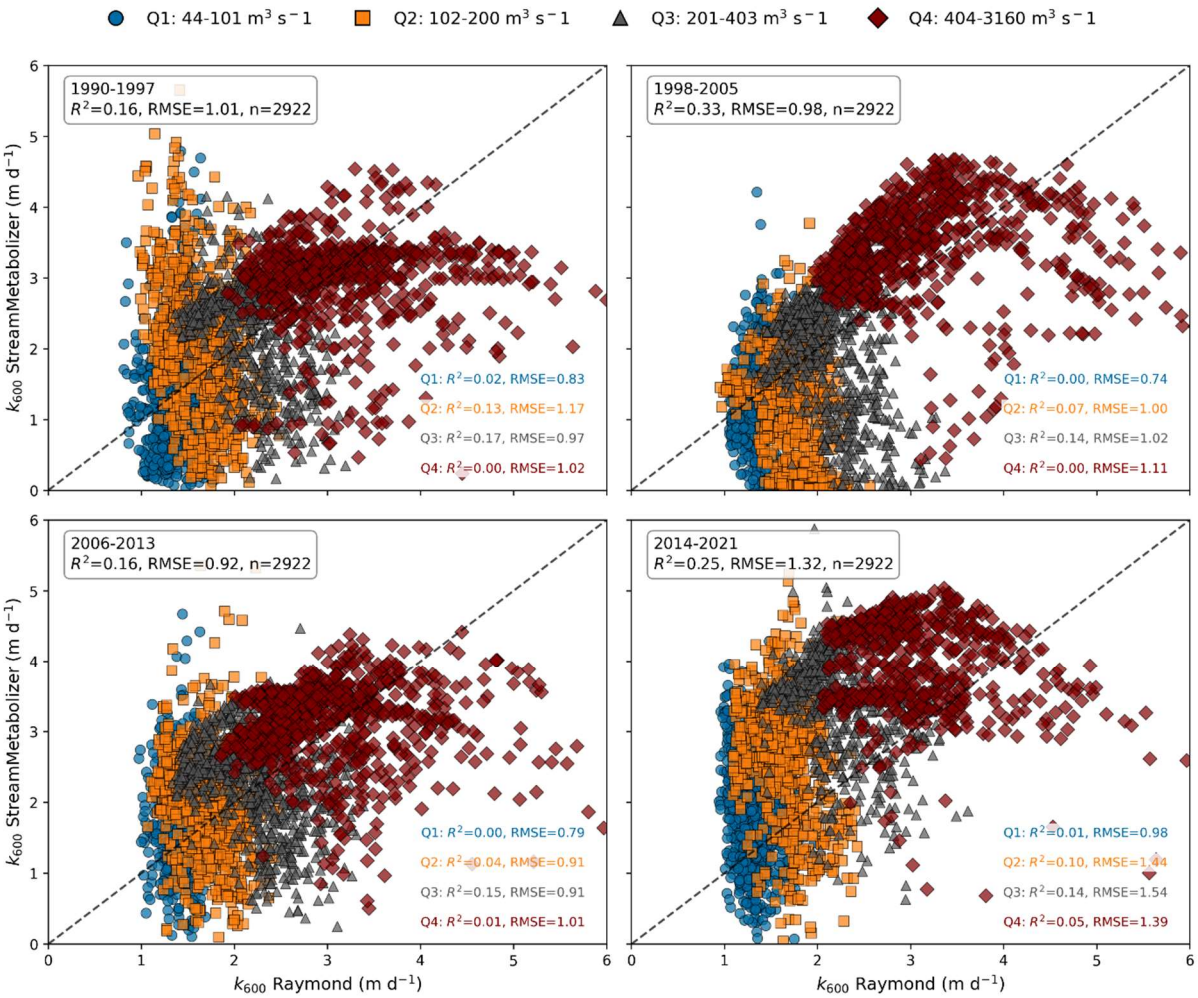

Figure B4. Compare the k600 between the mean of seven equations, Raymond et al. 2012, and StreamMetabolizer for 1990-2021. Colors indicate discharge quantiles (Q1-Q4, legend above). R^2 and RMSE are shown per discharge quantile range.

B3. Uncertainty Analysis

Estimating FCO_2 and NEP using models such as $PyCO_2SYS$ and streamMetabolizer often involves large uncertainties, particularly when considering the propagation of errors in all model input data and the summing/multiplying of these uncertainties in calculating fluxes (Battin et al., 2023; Kirk & Cohen, 2023). Estimating FCO_2 and NEP involves uncertainties from multiple sources. While a full error propagation was beyond the scope of this study, we assessed the impact of the largest source of input uncertainty: the reconstruction of daily TA, which was based on daily conductivity. The error in TA could potentially affect conclusions regarding the temporal distribution of CO_2 sink/source states throughout the year, as well as comparisons with NEP.

The average error in the reconstructed TA was ±190 µmol/L. Propagating this uncertainty through the $pyCO_2SYS$ model resulted in an uncertainty of ±11% in the final pCO_2 estimates. As shown in Table B1, this level of uncertainty did not alter the main conclusions of the study. The annual distribution of

trophic states remains consistent, with a maximum deviation of only 3% fluxes. Moreover, the dominance of the CO_2 source–heterotrophic state throughout the year remains almost unchanged, with less than a 1% difference under any range of TA uncertainty, though the magnitude of FCO_2 could vary up to 602 to 841 gC m^{-2} y^{-1}.

Table B1. Impact of TA uncertainty on the occurrence and FCO_2 of each trophlux state.

	Period	CO_2 source						CO_2 sink					
		Heterotrophic			Autotrophic			Heterotrophic			Autotrophic		
		Min	Mean	Max	Min	Mean	Max	Min	Mean	Max	Min	Mean	Max
% of days	1990-2000	47	47	48	16	17	18	8	7	7	30	29	28
	2001-2010	60	61	61	24	25	27	2	2	2	14	16	13
	2011-2021	65	66	66	25	26	28	1	1	1	9	7	6
FCO_2 (gC m^{-2} y^{-1}.)	1990-2000	831	954	1100	87	103	119	-5	-4	-4	-22	-21	-20
	2001-2010	1267	1454	1669	75	88	102	-1.3	-0.6	-1	-7.4	-7.8	-6.6
	2011-2021	602	717	841	49	59	71	-1.5	-0.9	-1.2	-3.4	-2.6	-2.1

B4. Methodological considerations for the Heterotrophic-Sink State

The Heterotrophic-Sink state (NEP < 0, FCO_2 < 0) represents a condition where the river is a net CO_2 sink from the atmosphere despite ongoing net ecosystem respiration. As discussed in the main text, we primarily attribute this transient state to significant CO_2 undersaturation in the water column resulting from intense prior autotrophic uptake. A recent analysis by Diamond et al. (2025) using this same dataset provides strong evidence for this mechanism. They found that heterotrophic-sink events were temporary, lasting an average of 4.7 ± 4.1 days, and that 76% of these events were immediately preceded by an autotrophic-sink state. This confirms our interpretation that the heterotrophic-sink state is not a stable condition but rather a short-lived transitionary phase as the river shifts from being an autotrophic-sink to either an autotrophic-source or a heterotrophic-source state. An additional potential contributing factor is the possible underestimation of GPP by the diel oxygen method. If oxygen produced within dense benthic macrophyte beds does not fully mix into the water column on a diel timescale, the reach-integrated GPP would be underestimated. This would result in a calculated NEP that is more negative than the true value, which could contribute to the Heterotrophic-Sink state.

Appendix C: Statistical Analyses of Long-Term Trends

This appendix provides detailed results from the statistical analyses used to identify and quantify the long-term changes discussed in the main text.

C1. Change-Point Analysis

We evaluated the long-term changes in FCO_2 and metabolism using a statistical change point analysis, which identifies points in a time series where the statistical properties, such as the mean or variance, undergo significant shifts. We first applied seasonal decomposition on daily time series to extract trend, seasonal, and residual components using the *statsmodels* Python package (Seabold & Perktold, 2010).

The long-term trend component was analyzed using a piecewise linear regression method (model ="linear" in *ruptures,* a Python package), while shift point detection by standard deviation (changes in variance by model="normal" in *ruptures*) was employed for the seasonal components. This process was also applied to related parameters, including daily discharge, temperature, GPP, and ER. The results of this analysis (Figure C1) informed the division of the 32-year record into the three decadal periods used for comparison throughout the manuscript.

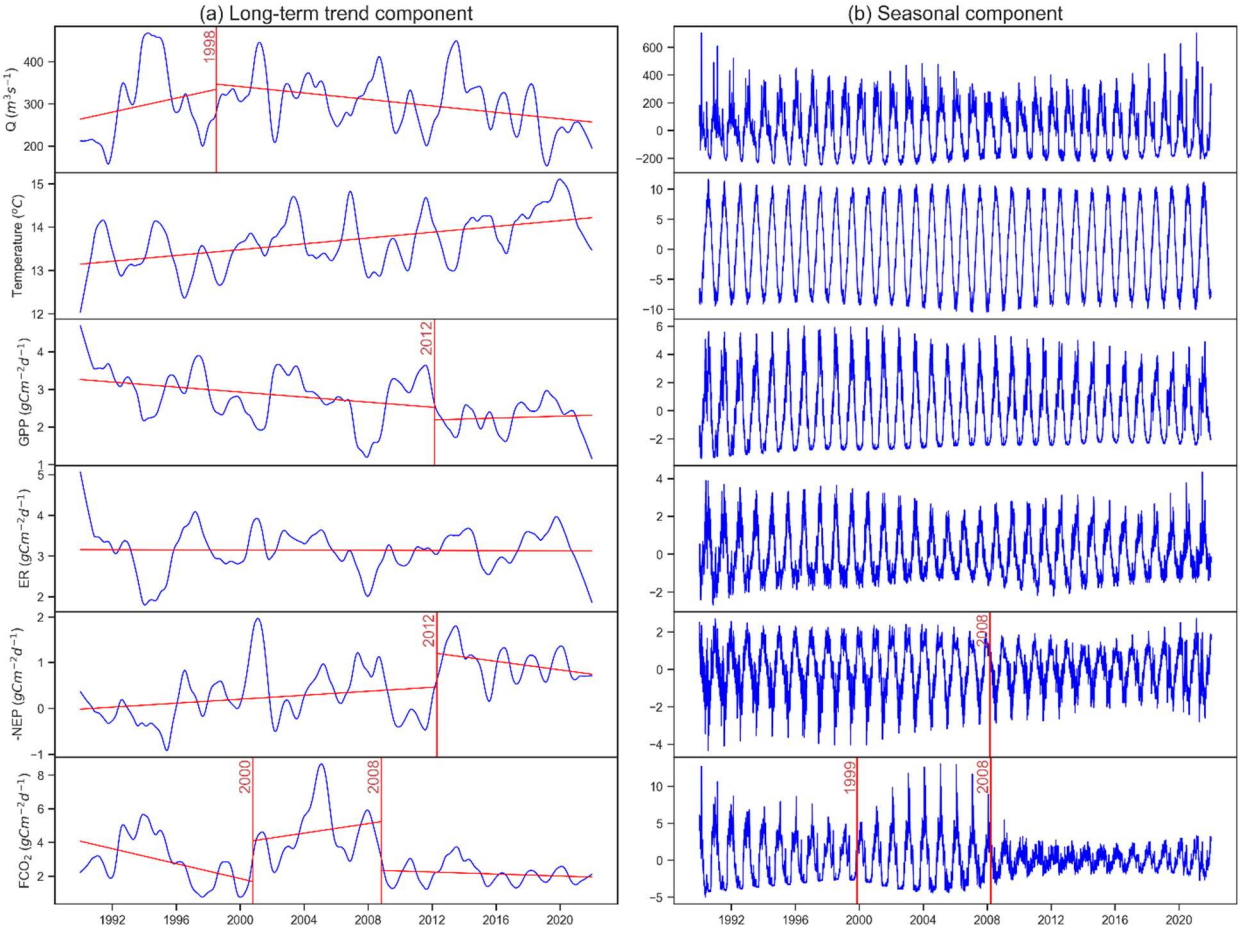

Figure C1. Change-point analysis on the decomposed time series: (a) long-term trend components and (b) seasonal components of daily discharge, temperature, and fluxes of GPP, ER, -NEP, and FCO_2. The red vertical lines indicate the change periods.

C2. Inter-Decadal Statistical Comparisons

To quantitatively assess differences between the three identified decades, we performed non-parametric Kruskal-Wallis tests followed by post-hoc Mann-Whitney U tests. The results (Figure C2) provide statistical validation for the observed shifts in key variables between the decadal periods.

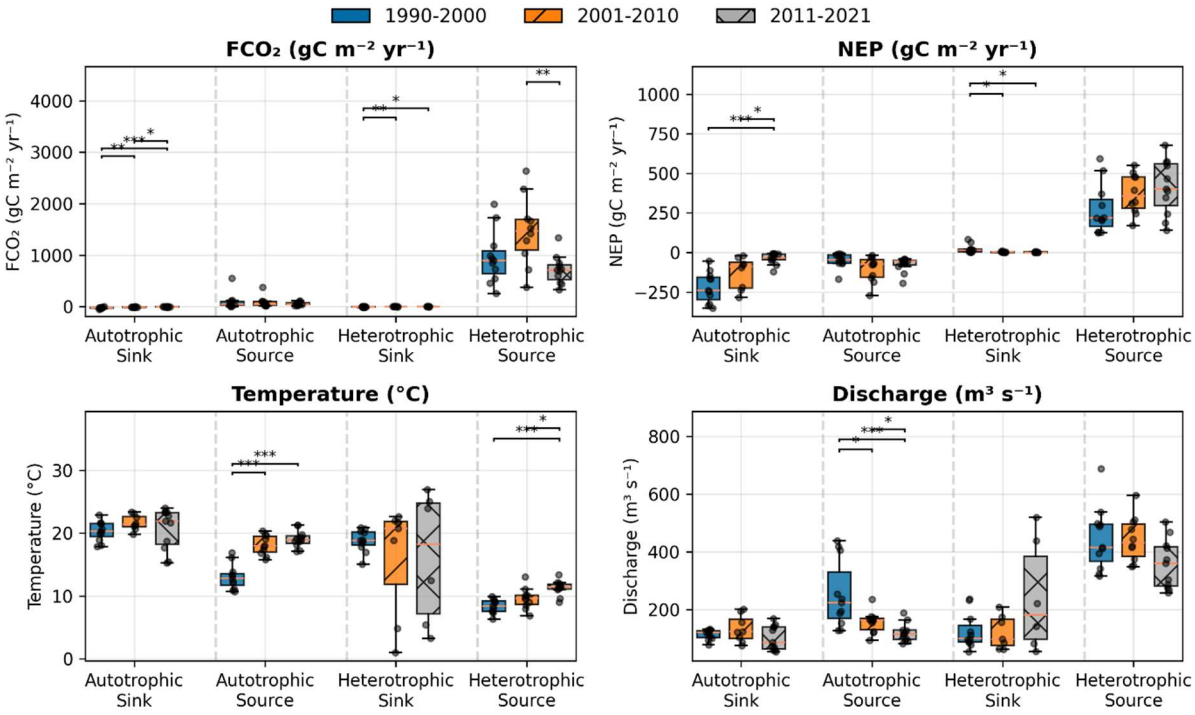

Figure C2. Statistical comparison of key variables across decades within each trophlux. Boxplots show median (horizontal line), interquartile range (box), and distribution of annual values (black dots). Colored boxes represent different decades: blue (1990-2000), purple (2001-2010), and orange (2011-2021). Statistical significance of differences between decades was assessed using Kruskal-Wallis tests, with significant pairwise differences (Mann-Whitney U test) indicated by horizontal bars with asterisks (* $p<0.05$, ** $p<0.01$, *** $p<0.001$).

Appendix D: Analysis of Hydroclimatic and External Drivers on FCO_2

This appendix presents the analyses that explore the potential drivers behind the observed long-term trends, particularly the decline in external CO_2 sources.

Table D1. The correlations (R^2) between annual FCO_2, -NEP, and hydroclimatic conditions (discharge, temperature) in each trophlux state

Trophlux	Parameters	Days	Discharge	Temp	FCO_2	-NEP	-NEP/CO_2
Autotrophic Sink	**Days**		0.08	0.01	0.07	0.14	0.00
	Discharge	0.08		0.07	0.19	0.03	0.19
	Temp	0.01	0.07		0.04	0.00	0.00
	FCO_2	0.07	0.19	0.04		0.14	0.32
	-NEP	0.14	0.03	0.00	0.14		0.13
	-NEP/CO_2	0.00	0.19	0.00	0.32	0.13	

Autotrophic Source	**Days**		0.00	0.06	0.06	0.16	0.00
	Discharge	0.00		0.34	0.41	0.00	0.36
	Temp	0.06	0.34		0.14	0.00	0.21
	FCO_2	0.06	0.41	0.14		0.13	0.32
	-NEP	0.16	0.00	0.00	0.13		0.01
	-NEP/CO_2	0.00	0.36	0.21	0.32	0.01	
Heterotrophic Sink	**Days**		0.01	0.21	0.00	0.03	0.05
	Discharge	0.01		0.40	0.67	0.00	0.16
	Temp	0.21	0.40		0.40	0.10	0.90
	FCO_2	0.00	0.67	0.40		0.01	0.18
	-NEP	0.03	0.00	0.10	0.01		0.12
	-NEP/CO_2	0.05	0.16	0.90	0.18	0.12	
Heterotrophic Source	**Days**		0.00	0.69	0.01	0.30	0.07
	Discharge	0.00		0.04	0.36	0.11	0.11
	Temp	0.69	0.04		0.09	0.07	0.06
	FCO_2	0.01	0.36	0.09		0.06	0.59
	-NEP	0.30	0.11	0.07	0.06		0.04
	-NEP/CO_2	0.07	0.11	0.06	0.59	0.04	

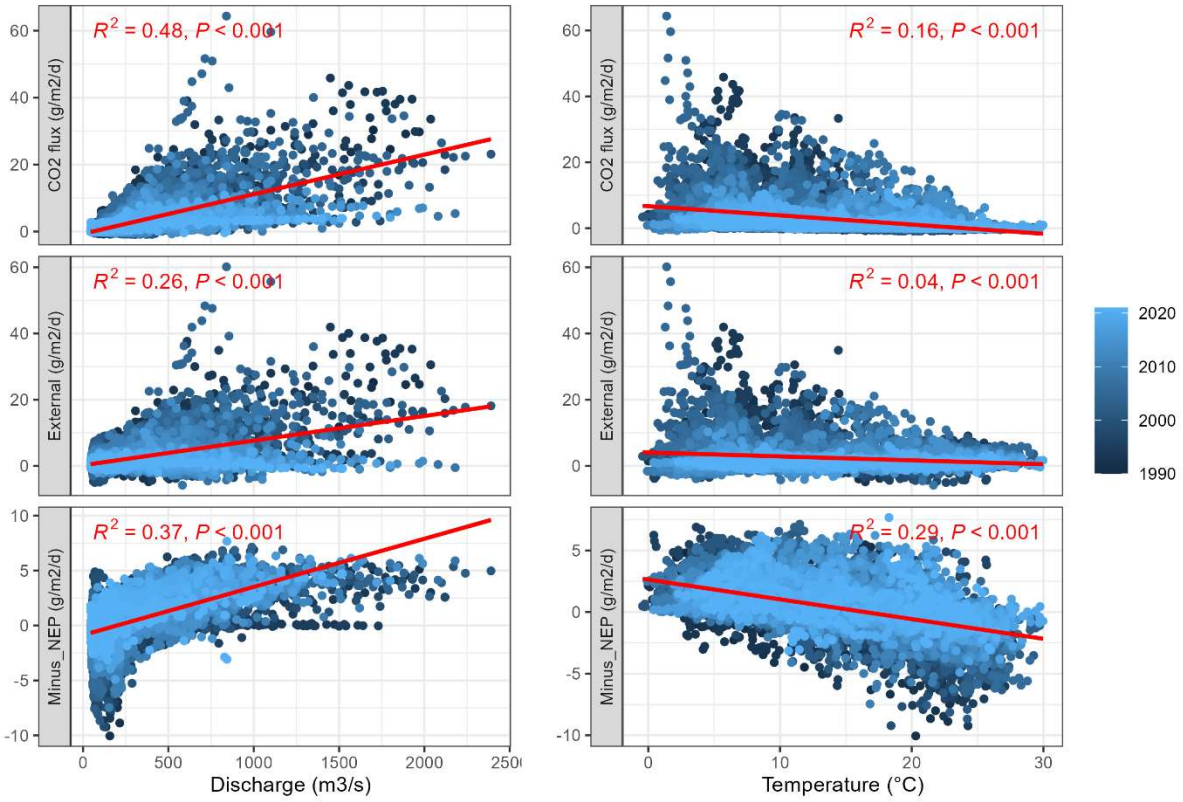

Figure D1. Relationship of daily fluxes and daily discharge or daily water temperature. Points are colored by year, as indicated by the color bar.

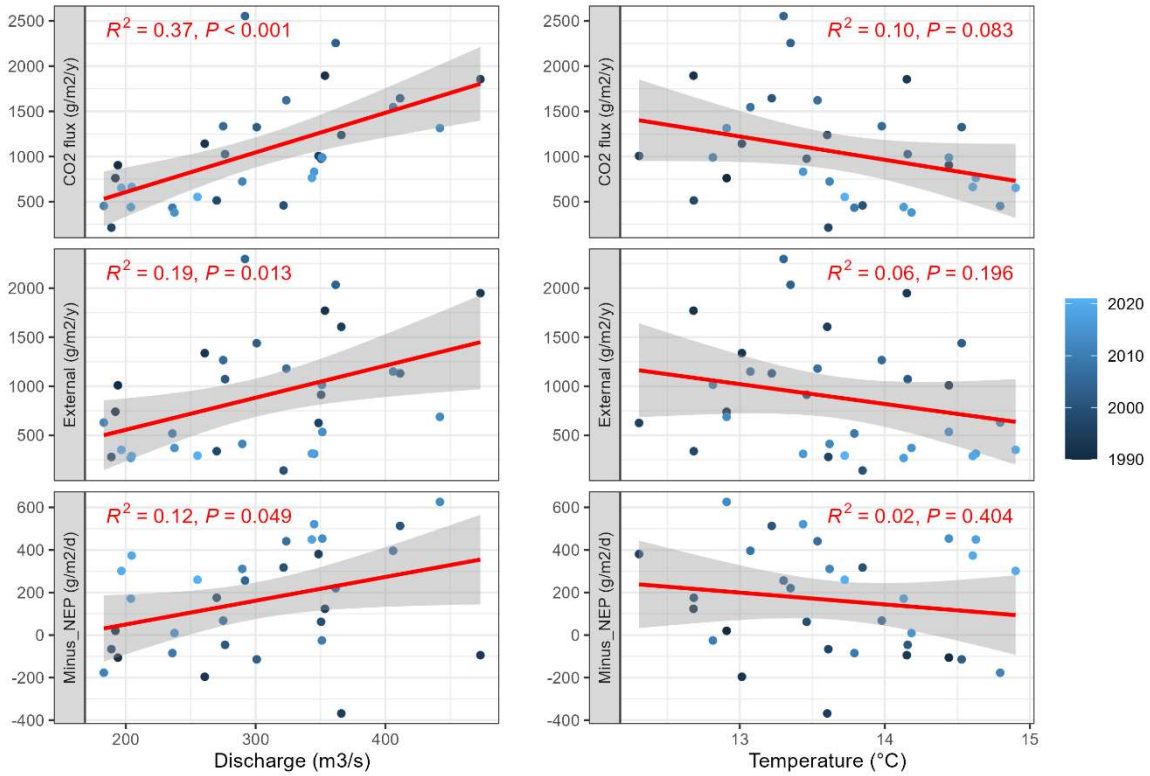

790

791 Figure D2. Relationship of annual fluxes and annual discharge or annual water temperature. Points are
792 colored by year, as indicated by the color bar.

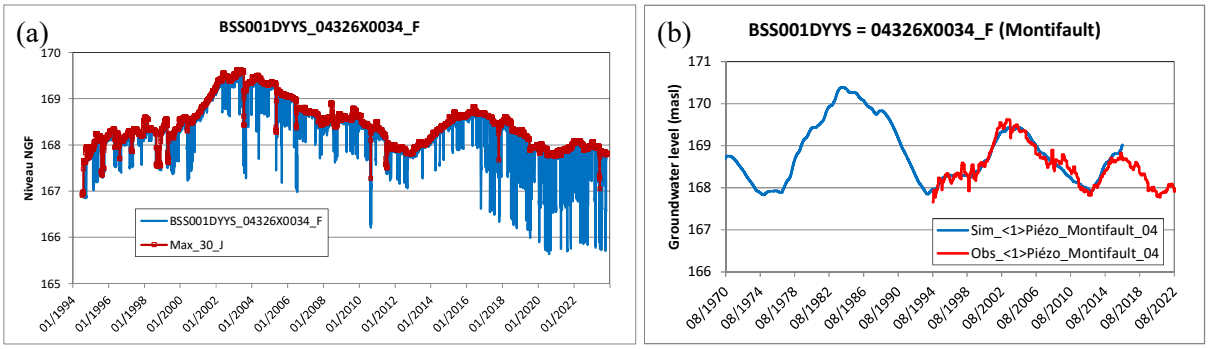

793

794 Figure D3. A decreasing trend in the groundwater level in Montifault (20 km from the study site). (a)
795 raw data, (b) after removing pumping effects with the EROS model (Data source: (Thiéry, 2018)).
796 NGF stands for "Nivellement Général de la France," which is the official vertical datum for France.

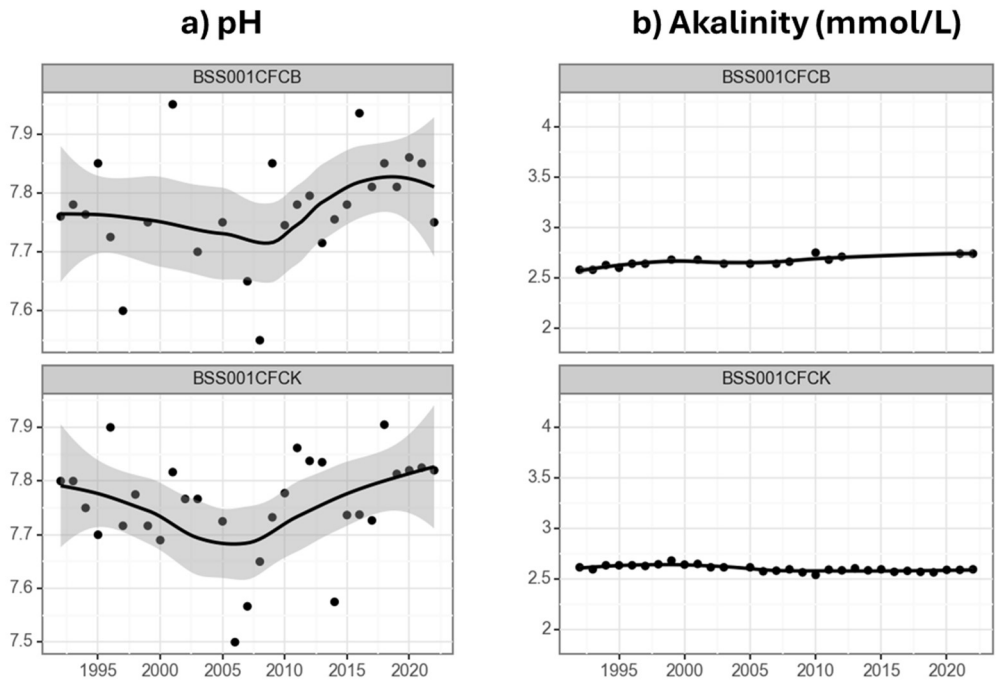

Figure D4. pH and alkalinity in groundwater monitoring stations in the vicinity (5 km radius) of the Dampierre study site (1990-2021). Points represent individual measurements, and solid lines are LOESS smoothers with 95% confidence intervals (shaded areas). Data source: https://hubeau.eaufrance.fr/page/api-qualite-nappes

Data availability

The hourly temperature, conductivity, dissolved oxygen, and pH data used in this study are owned by Électricité de France (EDF). Due to EDF's data-sharing policy, these data are not publicly available but can be accessed upon reasonable request by contacting EDF directly. Other publicly available datasets used include discharge (https://www.hydro.eaufrance.fr), river water quality (www.naiades.eaufrance.fr).

Author Contribution

ANT led the manuscript effort. ANT, JSD, GA, and FM came up with the research question and designed the study approach. ANT and JSD conducted the data curation and preparation, and ANT conducted the statistical analyses. ANT wrote the paper with contributions from all authors.

Competing interests

The authors declare that they have no known competing financial interests or personal relationships that could have appeared to influence the work reported in this paper.

Acknowledgements

We express our gratitude to Electricité de France (EDF) for generously providing us with extensive long-term datasets in the Middle Loire River.

References

Abril, G., & Borges, A. V. (2019). Ideas and perspectives: Carbon leaks from flooded land: Do we need to replumb the inland water active pipe? Biogeosciences, 16(3), 769–784. https://doi.org/10.5194/bg-16-769-2019

Abril, G., Bouillon, S., Darchambeau, F., Teodoru, C. R., Marwick, T. R., Tamooh, F., Ochieng Omengo, F., Geeraert, N., Deirmendjian, L., Polsenaere, P., & Borges, A. V. (2015). Technical note: Large overestimation of pCO2 calculated from pH and alkalinity in acidic, organic-rich freshwaters. Biogeosciences, 12(1), 67–78. https://doi.org/10.5194/bg-12-67-2015

Aho, K. S., Hosen, J. D., Logozzo, L. A., McGillis, W. R., & Raymond, P. A. (2021). Highest rates of gross primary productivity maintained despite CO 2 depletion in a temperate river network. Limnology and Oceanography Letters, 6(4), 200–206. https://doi.org/10.1002/lol2.10195

Amaral, J., Suhett, A., Melo, S., & Farjalla, V. (2013). Seasonal variation and interaction of photodegradation and microbial metabolism of DOC in black water Amazonian ecosystems. Aquatic Microbial Ecology, 70(2), 157–168. https://doi.org/10.3354/ame01651

Appling, A. P., Hall, R. O., Yackulic, C. B., & Arroita, M. (2018). Overcoming Equifinality: Leveraging Long Time Series for Stream Metabolism Estimation. Journal of Geophysical Research: Biogeosciences, 123(2), 624–645. https://doi.org/10.1002/2017JG004140

Battin, T. J., Lauerwald, R., Bernhardt, E. S., Bertuzzo, E., Gener, L. G., Hall, R. O., Hotchkiss, E. R., Maavara, T., Pavelsky, T. M., Ran, L., Raymond, P., Rosentreter, J. A., & Regnier, P. (2023). River ecosystem metabolism and carbon biogeochemistry in a changing world. Nature, 613(7944), 449–459. https://doi.org/10.1038/s41586-022-05500-8

Baulon, L., Allier, D., Massei, N., Bessiere, H., Fournier, M., & Bault, V. (2022). Influence of low-frequency variability on groundwater level trends. Journal of Hydrology, 606, 127436. https://doi.org/10.1016/j.jhydrol.2022.127436

Bernal, S., Cohen, M. J., Ledesma, J. L. J., Kirk, L., Martí, E., & Lupon, A. (2022). Stream metabolism sources a large fraction of carbon dioxide to the atmosphere in two hydrologically contrasting headwater streams. Limnology and Oceanography, 67(12), 2621–2634. https://doi.org/10.1002/lno.12226

Binet, S., Charlier, J.-B., Jozja, N., Défarge, C., & Moquet, J.-S. (2022). Evidence of long term biogeochemical interactions in carbonate weathering: The role of planktonic microorganisms and riverine bivalves in a large fluviokarst system. Science of the Total Environment, 842, 156823. https://doi.org/10.1016/j.scitotenv.2022.156823

Blaszczak, J. R., Delesantro, J. M., Urban, D. L., Doyle, M. W., & Bernhardt, E. S. (2019). Scoured or suffocated: Urban stream ecosystems oscillate between hydrologic and dissolved oxygen extremes. Limnology and Oceanography, 64(3), 877–894.

Bogard, M. J., & Del Giorgio, P. A. (2016). The role of metabolism in modulating CO 2 fluxes in boreal lakes. Global Biogeochemical Cycles, 30(10), 1509–1525. https://doi.org/10.1002/2016GB005463

Butman, D., & Raymond, P. A. (2011). Significant efflux of carbon dioxide from streams and rivers in the united states. Nature Geoscience, 4(12), Article 12. https://doi.org/10.1038/ngeo1294

Camenen, B., Grabowski, R. C., Latapie, A., Paquier, A., Solari, L., & Rodrigues, S. (2016). On the estimation of the bed-material transport and budget along a river segment: Application to the Middle Loire River, France. Aquatic Sciences, 78(1), 71–81. https://doi.org/10.1007/s00027-015-0442-3

Cole, J. J., Cole, J. J., Caraco, N. F., & Caraco, N. F. (2001). Carbon in catchments: Connecting terrestrial carbon losses with aquatic metabolism. Marine and Freshwater Research, 52(1), 101. https://doi.org/10.1071/MF00084

Cole, J. J., Prairie, Y. T., Caraco, N. F., McDowell, W. H., Tranvik, L. J., Striegl, R. G., Duarte, C. M., Kortelainen, P., Downing, J. A., Middelburg, J. J., & Melack, J. (2007). Plumbing the global carbon cycle: Integrating inland waters into the terrestrial carbon budget. Ecosystems, 10(1), 171–184. https://doi.org/10.1007/s10021-006-9013-8

Coynel, A., Etcheber, H., Abril, G., Maneux, E., Dumas, J., & Hurtrez, J.-E. (2005). Contribution of small mountainous rivers to particulate organic carbon input in the bay of biscay. Biogeochemistry, 74(2), 151–171.

Deirmendjian, L., & Abril, G. (2018). Carbon dioxide degassing at the groundwater-stream-atmosphere interface: Isotopic equilibration and hydrological mass balance in a sandy watershed. Journal of Hydrology, 558, 129–143. https://doi.org/10.1016/j.jhydrol.2018.01.003

Diamond, J. S., Bernal, S., Boukra, A., Cohen, M. J., Lewis, D., Masson, M., Moatar, F., & Pinay, G. (2021). Stream network variation in dissolved oxygen: Metabolism proxies and biogeochemical controls. Ecological Indicators, 131(September), 108233. https://doi.org/10.1016/j.ecolind.2021.108233

Diamond, J. S., Moatar, F., Cohen, M. J., Poirel, A., Martinet, C., Maire, A., & Pinay, G. (2022). Metabolic regime shifts and ecosystem state changes are decoupled in a large river. Limnology and Oceanography, 67(S1). https://doi.org/10.1002/lno.11789

Diamond, J. S., Truong, A. N., Abril, G., Bertuzzo, E., Chanudet, V., Lamouroux, R., & Moatar, F. (2025). Inorganic carbon dynamics and their relation to autotrophic community regime shift over three decades in a large, alkaline river. Limnology and Oceanography, n/a(n/a). https://doi.org/10.1002/lno.70016

Dodds, W. K., & Smith, V. H. (2016). Nitrogen, phosphorus, and eutrophication in streams. Inland Waters, 6(2), 155–164. https://doi.org/10.5268/IW-6.2.909

Duvert, C., Butman, D. E., Marx, A., Ribolzi, O., & Hutley, L. B. (2018). CO2 evasion along streams driven by groundwater inputs and geomorphic controls. Nature Geoscience, 11(11), Article 11. https://doi.org/10.1038/s41561-018-0245-y

Etcheber, H., Taillez, A., Abril, G., Garnier, J., Servais, P., Moatar, F., & Commarieu, M.-V. (2007). Particulate organic carbon in the estuarine turbidity maxima of the gironde, loire and seine estuaries: Origin and lability. Hydrobiologia, 588(1), 245–259. https://doi.org/10.1007/s10750-007-0667-9

Floury, M., Delattre, C., Ormerod, S. J., & Souchon, Y. (2012). Global versus local change effects on a large european river. Science of the Total Environment, 441, 220–229. https://doi.org/10.1016/j.scitotenv.2012.09.051

He, H., Wang, Y., Liu, Z., Bao, Q., Wei, Y., Chen, C., & Sun, H. (2022). Lake metabolic processes and their effects on the carbonate weathering CO2 sink: Insights from diel variations in the hydrochemistry of a typical karst lake in SW china. Water Research, 222, 118907. https://doi.org/10.1016/j.watres.2022.118907

Hotchkiss, E. R., Hall Jr, R. O., Sponseller, R. A., Butman, D., Klaminder, J., Laudon, H., Rosvall, M., & Karlsson, J. (2015). Sources of and processes controlling CO2 emissions change with the size of streams and rivers. Nature Geoscience, 8(9), 696–699. https://doi.org/10.1038/ngeo2507

Humphreys, M. P., Lewis, E. R., Sharp, J. D., & Pierrot, D. (2022). PyCO2SYS v1.8: Marine carbonate system calculations in python. Geoscientific Model Development, 15(1), 15–43. https://doi.org/10.5194/gmd-15-15-2022

Hussain, Md., & Mahmud, I. (2019). pyMannKendall: A python package for non parametric mann kendall family of trend tests. Journal of Open Source Software, 4(39), 1556. https://doi.org/10.21105/joss.01556

Ibáñez, C., Caiola, N., Barquín, J., Belmar, O., Benito, X., Casals, F., Fennessy, S., Hughes, J., Palmer, M., Peñuelas, J., Romero, E., Sardans, J., & Williams, M. (2022). Ecosystem-level effects of re-oligotrophication and N:P imbalances in rivers and estuaries on a global scale. Global Change Biology, n/a(n/a). https://doi.org/10.1111/gcb.16520

Janssen, P., Chevalier, R., Chantereau, M., Dupré, R., Evette, A., Hémeray, D., Mårell, A., Martin, H., Rodrigues, S., Villar, M., & Greulich, S. (2023). Can vegetation clearing operations and reprofiling of bars be considered as an ecological restoration measure? Lessons from a 10-year vegetation monitoring program (loire river, france). Restoration Ecology, 31(3), e13704. https://doi.org/10.1111/rec.13704

Jones, A. S., Jones, T. L., & Horsburgh, J. S. (2022). Toward automating post processing of aquatic sensor data. Environmental Modelling and Software, 151, 105364. https://doi.org/10.1016/j.envsoft.2022.105364

Jones, J. B., Stanley, E. H., & Mulholland, P. J. (2003). Long-term decline in carbon dioxide supersaturation in rivers across the contiguous united states. Geophysical Research Letters, 30(10), 2003GL017056. https://doi.org/10.1029/2003GL017056

Kirk, L., & Cohen, M. J. (2023). River corridor sources dominate CO2 emissions from a lowland river network. Journal of Geophysical Research: Biogeosciences, 128(1), e2022JG006954. https://doi.org/10.1029/2022JG006954

Koehler, B., Landelius, T., Weyhenmeyer, G. A., Machida, N., & Tranvik, L. J. (2014). Sunlight-induced carbon dioxide emissions from inland waters. Global Biogeochemical Cycles, 28(7), 696–711. https://doi.org/10.1002/2014GB004850

Liu, S., Kuhn, C., Amatulli, G., Aho, K., Butman, D. E., Allen, G. H., Lin, P., Pan, M., Yamazaki, D., Brinkerhoff, C., Gleason, C., Xia, X., & Raymond, P. A. (2022). The importance of hydrology in routing terrestrial carbon to the atmosphere via global streams and rivers. Proceedings of the National Academy of Sciences, 119(11), e2106322119. https://doi.org/10.1073/pnas.2106322119

Lynch, J. K., Beatty, C. M., Seidel, M. P., Jungst, L. J., & DeGrandpre, M. D. (2010). Controls of riverine CO 2 over an annual cycle determined using direct, high temporal resolution p CO 2 measurements. Journal of Geophysical Research: Biogeosciences, 115(G3), 2009JG001132. https://doi.org/10.1029/2009JG001132

Millero, F. J. (1979). The thermodynamics of the carbonate system in seawater. Geochimica et Cosmochimica Acta, 43(10), 1651–1661. https://doi.org/10.1016/0016-7037(79)90184-4

Minaudo, C., Meybeck, M., Moatar, F., Gassama, N., & Curie, F. (2015). Eutrophication mitigation in rivers: 30 years of trends in spatial and seasonal patterns of biogeochemistry of the loire river (1980–2012). Biogeosciences, 12(8), 2549–2563. https://doi.org/10.5194/bg-12-2549-2015

Moatar, F., Descy, J.-P., Rodrigues, S., Souchon, Y., Floury, M., Grosbois, C., Minaudo, C., Leitao, M., Wantzen, K. M., & Bertrand, F. (2022). Chapter 7—The loire river basin. In K. Tockner, C. Zarfl, & C. T. Robinson (Eds.), Rivers of Europe (Second Edition) (pp. 245–271). Elsevier. https://doi.org/10.1016/B978-0-08-102612-0.00007-9

Moatar, F., Fessant, F., & Poirel, A. (1999). pH modelling by neural networks. Application of control and validation data series in the middle loire river. Ecological Modelling, 120(2–3), 141–156. https://doi.org/10.1016/S0304-3800(99)00098-8

Moatar, F., & Meybeck, M. (2005). Compared performances of different algorithms for estimating annual nutrient loads discharged by the eutrophic River Loire. Hydrological Processes, 19(2), 429–444. https://doi.org/10.1002/hyp.5541

Moatar, F., Miquel, J., & Poirel, A. (2001). A quality-control method for physical and chemical monitoring data. Application to dissolved oxygen levels in the river loire (france). Journal of Hydrology, 252(1–4), 25–36. https://doi.org/10.1016/S0022-1694(01)00439-5

NOAA. (n.d.). Trends in atmospheric carbon dioxide. Global Monitoring Laboratory - Carbon Cycle Greenhouse Gases. https://gml.noaa.gov/ccgg/trends/data.html

Odum, H. T. (1956). Primary Production in Flowing Waters. Limnology and Oceanography, 1(2), 102–117. https://doi.org/10.4319/lo.1956.1.2.0102

Raymond, P. A., Caraco, N. F., & Cole, J. J. (1997). Carbon dioxide concentration and atmospheric flux in the hudson river. Estuaries, 20(2), 381. https://doi.org/10.2307/1352351

Raymond, P. A., Hartmann, J., Lauerwald, R., Sobek, S., McDonald, C., Hoover, M., Butman, D., Striegl, R., Mayorga, E., Humborg, C., Kortelainen, P., Dürr, H., Meybeck, M., Ciais, P., & Guth, P. (2013). Global carbon dioxide emissions from inland waters. Nature, 503(7476), 355–359. https://doi.org/10.1038/nature12760

Raymond, P. A., Zappa, C. J., Butman, D., Bott, T. L., Potter, J., Mulholland, P., Laursen, A. E., McDowell, W. H., & Newbold, D. (2012a). Scaling the gas transfer velocity and hydraulic geometry in streams and small rivers. Limnology and Oceanography: Fluids and Environments, 2(1), 41–53. https://doi.org/10.1215/21573689-1597669

Raymond, P. A., Zappa, C. J., Butman, D., Bott, T. L., Potter, J., Mulholland, P., Laursen, A. E., McDowell, W. H., & Newbold, D. (2012b). Scaling the gas transfer velocity and hydraulic geometry in streams and small rivers. Limnology and Oceanography: Fluids and Environments, 2(1), 41–53. https://doi.org/10.1215/21573689-1597669

Reed, A. P., Stets, E. G., Murphy, S. F., & Mullins, E. A. (2021). Aquatic-terrestrial linkages control metabolism and carbon dynamics in a mid-sized, urban stream influenced by snowmelt. Journal of Geophysical Research: Biogeosciences, 126(9), e2021JG006296. https://doi.org/10.1029/2021JG006296

Rocher-Ros, G., Harms, T. K., Sponseller, R. A., Väisänen, M., Mörth, C.-M., & Giesler, R. (2021). Metabolism overrides photo-oxidation in CO2 dynamics of Arctic permafrost streams. Limnology and Oceanography, 66(S1), S169–S181. https://doi.org/10.1002/lno.11564

Rocher-Ros, G., Sponseller, R. A., Bergström, A., Myrstener, M., & Giesler, R. (2020). Stream metabolism controls diel patterns and evasion of CO 2 in arctic streams. Global Change Biology, 26(3), 1400–1413. https://doi.org/10.1111/gcb.14895

Seabold, S., & Perktold, J. (2010). Statsmodels: Econometric and statistical modeling with python. 92–96. https://doi.org/10.25080/Majora-92bf1922-011

Solano, V., Duvert, C., Birkel, C., Maher, D. T., García, E. A., & Hutley, L. B. (2023). Stream respiration exceeds CO_2 evasion in a low-energy, oligotrophic tropical stream. Limnology and Oceanography, 68(5), 1132–1146. https://doi.org/10.1002/lno.12334

Thiéry, D. (2018). EROS: A semi-global hydrological modelling application for a catchment area divided into sub-basins | BRGM. https://www.brgm.fr/en/software/eros-semi-global-hydrological-modelling-application-catchment-area-divided-sub-basins

Trentman, M. T., Hall, R. O., & Valett, H. M. (2023). Exploring the mismatch between the theory and application of photosynthetic quotients in aquatic ecosystems. Limnology and Oceanography Letters. https://doi.org/10.1002/lol2.10326

Truong, C., Oudre, L., & Vayatis, N. (2020). Selective review of offline change point detection methods. Signal Processing, 167, 107299. https://doi.org/10.1016/j.sigpro.2019.107299

Tsypin, M., & Macpherson, G. L. (2012). The effect of precipitation events on inorganic carbon in soil and shallow groundwater, konza prairie LTER site, NE kansas, USA. Applied Geochemistry, 27(12), 2356–2369. https://doi.org/10.1016/j.apgeochem.2012.07.008

Van Vliet, M. T. H., Franssen, W. H. P., Yearsley, J. R., Ludwig, F., Haddeland, I., Lettenmaier, D. P., & Kabat, P. (2013). Global river discharge and water temperature under climate change. Global Environmental Change, 23(2), 450–464. https://doi.org/10.1016/j.gloenvcha.2012.11.002

Vihermaa, L. E., Waldron, S., Garnett, M. H., & Newton, J. (2014). Old carbon contributes to aquatic emissions of carbon dioxide in the Amazon. Biogeosciences, 11(13), 3635–3645. https://doi.org/10.5194/bg-11-3635-2014

Wallin, M. B., Audet, J., Peacock, M., Sahlée, E., & Winterdahl, M. (2020). Carbon dioxide dynamics in an agricultural headwater stream driven by hydrology and primary production. Biogeosciences, 17(9), 2487–2498. https://doi.org/10.5194/bg-17-2487-2020

Young, F. L., Colman, B. P., Carter, A. M., Fiejó De Lima, R., Shangguan, Q., Payn, R. A., & DeGrandpre, M. D. (2025). Variability and Controls of p CO2 and Air-Water CO2 Fluxes in a Temperate River. Journal of Geophysical Research: Biogeosciences, 130(2), e2024JG008434. https://doi.org/10.1029/2024JG008434

Zhang, T., Li, J., Pu, J., Martin, J. B., Khadka, M. B., Wu, F., Li, L., Jiang, F., Huang, S., & Yuan, D. (2017). River sequesters atmospheric carbon and limits the CO2 degassing in karst area, southwest China. Science of the Total Environment, 609, 92–101. https://doi.org/10.1016/j.scitotenv.2017.07.143